Degradation mechanisms of low-calcium fly ash-based geopolymer mortar in simulated aggressive sewer conditions

Piumika W. Ariyadasa [a], Allan C. Manalo [a,*], Weena Lokuge [a], Vasantha Aravienthan [b], Andreas Gerdes [c], Jonas Kaltenbach [c]

[a] *School of Engineering, Centre for Future Materials, University of Southern Queensland, Toowoomba 4350, Queensland, Australia*
[b] *School of Engineering, University of Southern Queensland, Toowoomba, 4350, Queensland, Australia*
[c] *Institute for Functional Surfaces, Karlsruhe Institute of Technology, Karlsruhe, Germany*

A R T I C L E   I N F O

A B S T R A C T

Alkali-activated geopolymers are increasingly studied as alternatives to Ordinary Portland Cement (OPC) concrete for use in challenging service environments. Low-calcium geopolymers have been advocated to mitigate Microbial-Induced Concrete Corrosion (MICC) in sewer pipes; however, their broader acceptance as a repair material for sewer rehabilitation remains to be established. This study evaluated the degradation mechanism of low-calcium fly ash-based geopolymer (FAGP) repair mortar under laboratory-simulated sewer conditions by exposing it to varying concentrations of sulphuric acid (pH 0.5, 1, and 4) for extended durations. The corrosion of the mortar samples was assessed based on visual changes, mass loss, residual mechanical strength, pore evolution, and ion transport over three exposure durations. Comparative analysis with OPC counterparts served as a benchmark. The degradation of FAGP and OPC due to acid exposure appears to escalate with both acid concentration and exposure. However, FAGP displayed superior performance by maintaining their shape and retaining approximately 30% of mechanical strength even after 3000 h of exposure under highly aggressive sewer conditions at pH 0.5. In contrast, OPC fails to endure acid exposure beyond 2000 h. The loss of matrix integrity primarily stems from ion leaching, supported by Scanning Electron Microscopy and Mercury Intrusion Porosimetry analysis, which revealed the creation of intrinsic pores facilitating the ingress of sulphate ions into the matrix. X-Ray Diffraction (XRD) and Fourier Transform Infrared (FTIR) Spectroscopy patterns indicate no significant phase alterations, confirming this phenomenon. In conclusion, this study demonstrated that FAGP mortar is more resilient and durable in mild to aggressive sewer conditions than OPC.

1. Introduction

Geopolymers, being clinker-free, offer a promising solution to the durability issues that traditional concrete materials marginally perform. This makes them a viable alternative for infrastructure projects exposed to chemically aggressive environments [1–3]. The comparison of geopolymer with traditional Portland cement-based concrete in sewer conditions is a critical area of research, given the durability challenges that concrete sewers face due to microbial-induced corrosion [4], incurring significant replacement or rehabilitation costs [5,6]. The mechanisms by which concrete deteriorates due to this biogenically produced sulphuric acid attack are complex, involving a chemo-transport-damage process [7]. This process begins with the intrusion of exogenous sulphate ions, disrupting the pore solution's equilibrium

condition in the concrete matrix [8]. This results in the dissolution of portlandite (CH) and the decalcification of calcium silicate hydrates (C-S-H), with consequent formation of expansive products such as gypsum and ettringite, followed by spalling, which reduces the integrity of the concrete matrix and renders the infrastructure unfit for use [9,10].

Many studies [11–13] have compared alkali-activated geopolymer to Ordinary Portland Cement (OPC) for use in hostile sewer conditions. Among the three test methodologies reported in the literature, i.e. in situ, laboratory chemical, and laboratory microbiological, some scientists [12,14–16] have strongly advocated comparing the performance of binder materials under laboratory conditions that simulate chemically induced sewer environments. Some argue that trials in chemically induced sewer conditions are unreliable because they only model a subset of probable events, such as the final phase of biologically induced

---

* Corresponding author.
  E-mail address: allan.manalo@usq.edu.au (A.C. Manalo).

acid attack, and do not reflect bacterial incubation or acid generation processes [17,18]. Damion and Chaunsali [19] and Gu et al. [20] have disputed this approach, stating that if the parameters of natural sewer conditions are inconsistent with the location, it is difficult to predict the durability performance of repair binders. Thus, it is difficult to reproduce the same conditions for research extensions. One of the primary benefits of chemically induced laboratory circumstances is that they allow for a more streamlined evaluation procedure with fewer variables to manage and can expedite the research for quick results [21]. This is especially useful for testing and comparing binder materials that create complex and different reaction products when exposed to sulphuric acid [22].

Sulphuric acid with a pH of 0.5 to 1 is widely employed in achieving chemically-induced binder degradation [6]. These acidic levels replicate aggressive sewer conditions; hence, this test approach is designated an expedited process [23]. Albitar et al. [24] and Khan et al. [25] reported the use of 3% and 1.5% (weight/weight) sulphuric acid, respectively, to simulate sewer conditions. They reported mass loss of 4.0% and 4.5% and strength loss of 11% and 25% for fly ash (FA)-based geopolymer and a combination of FA and ground granulated blast slag (GGBS) geopolymers, respectively. Gu et al. [21] tested alkali-activated geopolymer (AAC) in 3% (0.5 pH) sulphuric acid to accelerate the reaction under laboratory sewer conditions. They observed a 3% loss in mechanical strength for 116 days compared to the non-accelerated test run at 1% (1 pH) sulphuric acid, which took an extra month to exhibit comparable degradation. Geopolymer binders are intricate aluminosilicates whose composition varies depending on the tailing procedure. Thus, the reaction products of acid corrosion may have diverse results due to differences in their chemistry [26]. Exposure duration is another critical aspect in binder durability in aggressive conditions. Grengg et al. [27] conducted a performance study of metakaolin-based geopolymer exposed to microbially induced acid corrosion, comparing it with OPC-based materials over 18 months. Khan et al. [28] reported on a long-term durability study of geopolymers synthesised from FA and GGBS mixed at various percentages exposed to natural sewer conditions. Geopolymers with low levels of calcium (Ca) and aluminium (Al) appear to outperform in both cases, a consensus supported by numerous other researchers [12,29,30] due to expected low decalcification and, thus, low mass loss and mechanical strength loss. The geopolymer-based repair products currently available in the market have been found to be unfeasible in the long term, and this is primarily due to the residual calcium content in these materials, which contributes to deterioration when exposed to aggressive sewer environments [6]. However, little research has been conducted to evaluate the long-term performance of geopolymers made solely from low-calcium fly ash in aggressive conditions.

Most durability studies have focused on chemical damage, assessing residual mechanical properties and altered microstructures. Unfortunately, these studies neglected the effect of ion transport, which is crucial in comparing the effectiveness of binder materials for use in sewer conditions and, more importantly, as a liner material for sewer pipe rehabilitation [29]. According to laboratory findings [24,31] and field experience [32], the low-porosity matrix of materials, which can effectively obstruct or slow the transport process, primarily determines their endurance. Hence, the assumption of comparable pore structures in unexposed binder matrices may lead to incorrect conclusions when comparing binders based on their post-acid attack characteristics. The disparity in concentration is also a decisive factor in Fick's law of diffusion and capillary suction [33]. Thus, examining the impact of acid concentration on infiltration and the subsequent reaction that leads to geopolymer disintegration is imperative. This will assist in understanding mortar disintegration in various sewer environments. According to Madraszewski et al. [17], periodic acid replenishment in chemical-induced testing disrupts the corrosion process. This is extremely unlikely in natural sewer conditions where bacterial species thrive and continuously provide biogenic sulphuric acid to the corrosion process.

To address the abovementioned research gaps, this study assessed the degradation of fly ash-based geopolymer mortar under a range of exposure conditions for an extended period, simulating the sulphuric acid corrosion in aggressive sewer environments. Chemical-induced laboratory test conditions were implemented, wherein the sulphuric acid-deteriorated mortar was assessed through physico-mechanical properties, phase transition, alkali ion leaching, and microstructural evolution, with particular attention to correlating these with binder transport characteristics. Conventional OPC mortar was used to distinguish the geopolymer degradation mechanism and justify the imposed sewer conditions by comparing OPC deterioration rates to prior research conducted under comparable settings. In Australia, sewer trunk mains or reticulation mains with pipe diameters >225 mm are typically constructed from concrete, often incorporating a sacrificial layer to mitigate the material loss caused by inevitable biogenic acid corrosion. This rationale underpinned the use of OPC repair mortar in this study as a counterpart to geopolymer mortar. The inclusion of OPC mortar allowed for a comprehensive understanding of the severity of concrete corrosion in aggressive sewer conditions while also serving as a comparative benchmark to assess the effects of corrosion on low-calcium geopolymer mortar in terms of physical, mechanical, chemical, and pore structure changes. The outcomes of this study will provide a better understanding of the mechanisms and factors contributing to geopolymer degradation in sewer conditions. This insight will facilitate the development of a more resilient and sustainable alternative to OPC binder. Furthermore, these results can lead to advancements in repair and rehabilitation techniques for existing concrete infrastructure in different sewer conditions. Overall, the findings of this study will assist in enhancing the resilience, sustainability, and longevity of concrete structures, thereby contributing to the safety and functionality of the built environment.

2. Experimental methodology

2.1. Materials

This study employed a low-calcium FA as the mineral precursor for producing fly ash geopolymer (FAGP) repair mortar. The Class FA was activated using a combination of 16-molarity sodium hydroxide (SH) and sodium silicate (SS) solutions in a 1:2 ratio. Commercially available river sand (Quartz) was used as the fine aggregates (s) in the mortar, with the particle size <1.18 mm. Ordinary Portland Cement (OPC) mortar was employed as the counterpart in durability studies to simulate real-life scenarios in concrete sewers. The X-ray fluorescence (XRF) results, presented in Table 1, indicate that the calcium oxide content in FA and OPC is 3.8% and 57.3%, respectively.

2.2. Sample preparation

The methodology outlined by Ariyadasa et al. [6], was followed in preparing mortar specimens, where the alkali activator solution (AAS) to binder (FA + anhydrous activator) ratio was maintained at 0.55. The w/binder ratio applied was 0.37, where 'w' represents the water content from the NaOH solution and any additional pure water. Fine aggregates were added to the FAGP mortars at a sand-to-binder ratio of 2. OPC mortars were prepared by mixing cement, water and sand with a water-to-OPC ratio of 0.45 and a sand-to-OPC ratio of 1.5. Freshly mixed mortars of FAGP and OPC were cast into moulds, vibrated to eliminate air bubbles, and sealed with plastic wrap for 24 h of initial conditioning at ambient temperature (24 ± 2 °C). Following that, FAGP mortars were heat-cured for 24 h at 80 °C before being cured for 28 days under ambient conditions, whilst OPCs were maintained humid (Relative Humidity = 85%) until the test date. Previous research [34–36] suggested that OPC is highly susceptible to strong acid attacks. To ensure durability during the investigation, specimens measuring leaching ions were built 30 mm and 60 mm in diameter and height, respectively and

Table 1
Chemical composition of the raw binder materials.

Oxide(wt%)	SiO$_2$	Al$_2$O$_3$	Fe$_2$O$_3$	CaO	P$_2$O$_5$	TiO$_2$	MgO	K$_2$O	SO$_3$	MnO	Na$_2$O	LOI
Class F FA*	47.9	28.0	14.1	3.8	1.8	2.0	0.9	0.6	0.3	0.2	0.4	0.4
OPC*	20.6	7.2	3.9	57.3	0.1	0.4	4.7	0.8	4.4	0.1	0.2	_

LOI- Los of Ignition, [6]*.

30 mm by 30 mm elsewhere.

2.3. Experimental methodology

This study employed an accelerated chemical attack to simulate sewer conditions and evaluate the degradation of repair mortar when subjected to biogenic sulphuric (H$_2$SO$_4$) acid. The literature indicates that the surface pH of damaged concrete sewer pipes subjected to aggressive microbial corrosion (final stage) is <1 [36,37]. However, this study used an acid solution with a pH range of 0.5 to 4.0 to simulate both the middle and end stages of the corrosion process. Fig. 1 presents the submergence of FAGP and OPC mortar samples in H$_2$SO$_4$ solutions of 0.5, 1, and 4 pH for varying durations in separate containers. This is to maintain a consistent sample-to-solution ratio in every chamber. Then, the containers were kept in an oven at 40 °C throughout the study period. A portable digital pH tester was used to measure the pH of the sulphuric acid solution every three days. Acid solutions were replenished to prevent the H$^+$/OH$^-$ concentration from reaching equilibrium, resulting in the loss of reaction momentum and inhibiting the corrosion process [17]. Following each stage, the retrieved samples were assessed for the long-term performance of the repair material using physical, chemical, and mechanical tests. The study evaluated the test specimens' responses to varied acid concentrations and exposure times and compared them to control samples. To replicate dynamic flow in a sewer pipe, the specimens for the ion leaching test were kept in individual containers in an incubator (at 40 °C) agitated at 30 rpm. This prevents the accumulation of corrosion products on the mortar surface and obstructs the movement of corrosive ions from the acid solution to the intact core, reducing the corrosion rate [22]. The specimens exposed to acid are labelled with a specific format, where alphabetical characters represent the type of mortar, followed by the pH value of the acid solution, and then the duration of exposure. For instance, "FAGP_0.5pH_1000" denotes FAGP mortar samples immersed in a 0.5pH sulphuric acid solution for 1000 h. Fig. 1 illustrates the investigation procedure adopted in this study for the acid-exposed specimens. The degradation analysis involved a total of 323 samples, with 17 samples per specimen type, including control (17 samples: 2 for visual observation, 10 for mechanical strength tests, 1 for phase transition testing, 1 for pore analysis, and 3 for leaching tests).
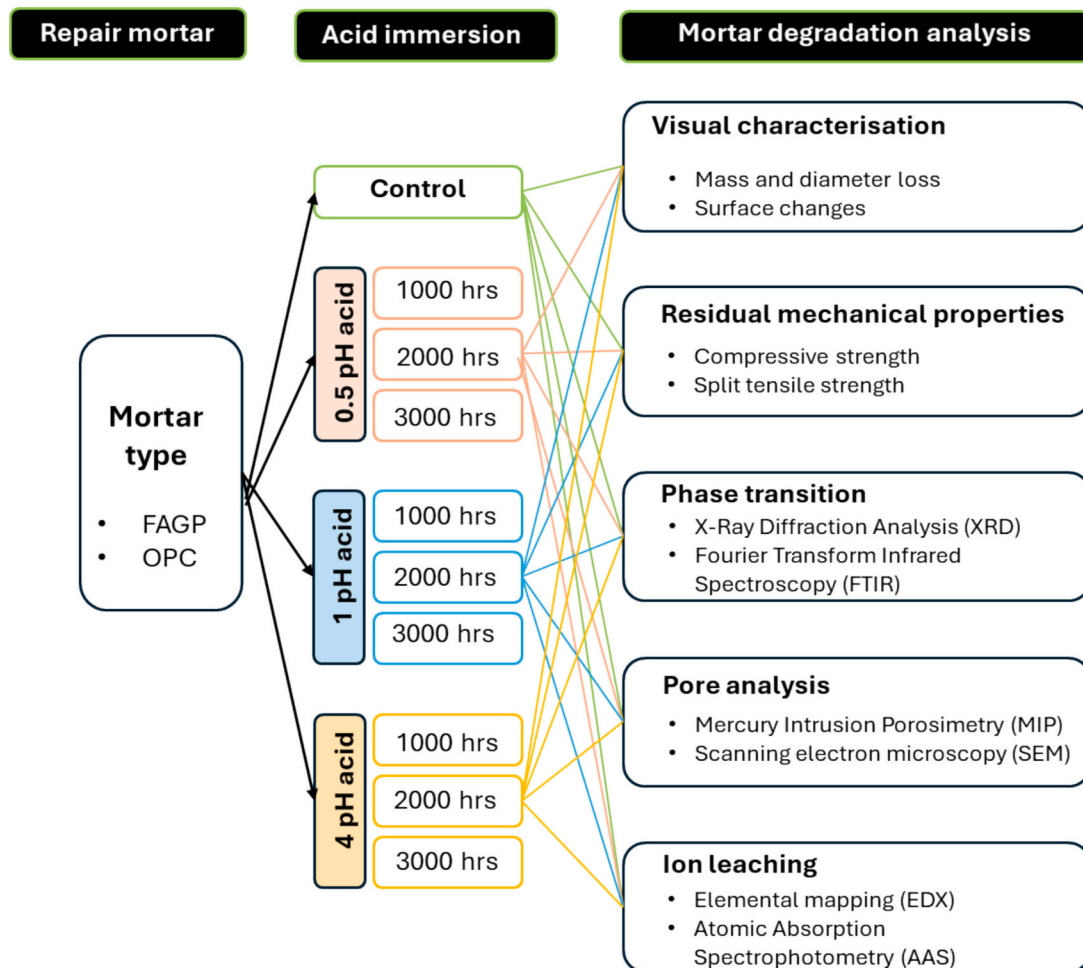

Fig. 1. Schematic diagram of the experimental methodology for the acid-exposed mortar specimens

2.3.1. Visual characterisation

This study employed an accelerated chemical attack to simulate sewer conditions. Before acid exposure, the 28-day-aged mortar specimens were measured for mass, cross-section, and height. After each immersion period, the specimens were removed from the acid solution, thoroughly cleaned with deionised water to remove any loose material, and then allowed to air dry for 48 h and oven dry for 24 h at 40° before being weighed. A Zeiss optical microscope (x 100 magnification) was used to evaluate colour changes, micro-cracking, and the extent of degradation in repair mortars.

2.3.2. Residual mechanical properties

Compressive and split tensile strength tests were used to characterise the hardened repair mortars. After each exposure cycle, the acid-deteriorated specimens were dried at 40 °C for 24 h before being evaluated in quadruplicate for residual compressive strength and split tensile strength following ASTM C109 [38] and ASTMC496/496 M [39], respectively, using a 100kN MTS Universal compression tester at a speed of 0.5 mm/min.

2.3.3. Phase transition

The phase evolution of acid-exposed repair mortars was investigated using X-ray diffraction (XRD) and Fourier transform infrared (FTIR) spectroscopy analyses. Samples were collected from the outer surface of the exposed mortar specimens (at the acid front) in the desired size and analysed as described below.

2.3.3.1. X-ray diffraction (XRD).
A D8 Advance Bruker diffractometer was used to monitor the mineralogical changes in the post-acid exposed mortar specimens. The samples were pulverised, sieved through a 75-μm sieve, and then examined through a High-speed LYNXEYE XE-T detector configured on Cu Kα-1.5405 λ at 40 kV and 100 mV. The diffractogram's scanning 2-theta range was 1°–150° with a scanning rate of 0.033 s for each 0.02° step. The diffractograms were analysed using the DIFFRAC. EVA program.

2.3.3.2. Fourier transform infrared (FTIR) spectroscopy.
For the FTIR spectroscopy measurements, samples from the deteriorated zone of the repair mortar were thoroughly dried before being crushed into fine powder. The IRAffinity-IS series SHIMADZU FT-IR spectrophotometer, with a wavelength range of 350 cm^{-1} to 7800 cm^{-1} and a maximum spectra resolution of 0.5 cm^{-1}, was used to detect changes in the functional groups of mortar species exposed to acid corrosion. The FTIR spectra of unexposed mortar samples were also collected for comparison.

2.3.4. Pore structure characteristics

2.3.4.1. Mercury intrusion porosimetry (MIP) analysis.
The porosity in mortar specimens was quantitatively assessed before and after exposure to acid using a fully automated Thermo Fisher Scientific PASCA 440EVO porosimeter. Samples were placed into the mercury intrusion porosimeter for vacuum-assisted degassing to prepare for pore analysis.

2.3.4.2. Scanning electron microscopy (SEM) analysis.
A TESCAN VEGA 111 SEM microscope with EDX was used at 25 keV to analyse concrete microstructure and composition. Low-vacuum imaging, which is advised for sensitive samples, was used. Full-sized specimens (30 mm diameter. Cross-section) were analysed to ensure a comprehensive assessment and to prevent sample damage from microcracks. The microscope's stitching capability enabled segmented analysis for rapid spot identification of microstructural variations, which aided in a detailed understanding of the mortar performance under sulphuric acid attack.

2.3.5. Ion leaching

2.3.5.1. Elemental distribution mapping.
The Energy Dispersive X-ray (EDX) Analysis elemental mapping approach was used to explore the distribution of elements within aged mortar samples. Various elements were mapped to qualitatively define the phases of corrosion products in the aged mortar samples compared to their unexposed counterparts. The non-destructive nature of the EDX enables the examination of heavily deteriorated specimens without requiring any sample preparation.

2.3.5.2. Atomic absorption spectrophotometry (AAS) analysis.
Mortar specimens of 30 mm diameter and 60 mm height were immersed in sulphuric acid solutions of different concentrations to investigate the extent of ion leaching due to acid attacks and stored in an incubator at 40 °C until each exposure period was completed. The suspensions were continuously stirred during exposure, and samples were collected at each acid replenishment time. The concentrations of Ca and aluminium ions in the leachate were measured using Atomic absorption spectrometry. All the leachates were stored at subzero temperatures until the test date, one day after each exposure cycle ended. The total ion leached at each exposure cycle was then measured and calculated.

3. Results and discussion

3.1. Physical characterisation

3.1.1. Mass/cross-section change

The dried specimens were sliced meticulously using an IsoMet 1000 precision saw; a 3 mm disc taken at the mid-height of each specimen was used for visual examination. Fig. 2 shows the macro-evolution of deteriorated mortar specimens exposed to sulphuric acid at different concentrations (pH levels of 0.5, 1, and 4). The cross-sections of FAGP and OPC specimens cut at half height are represented in (a) and (b), respectively.

In FAGP specimens exposed to sulphuric acid at 0.5pH, which represented the aggressive sewer condition, there was minimal to no change in specimen shape. However, a colour change was evident in FAGP specimens recovered after 1000 h of exposure, with up to one-third of the radius spread evenly, demarcating the acid front in a brown ring. Ariyadasa et al. [6] observed this phenomenon and reported a comparable occurrence in FAGP specimens exposed to 0.5pH acid for 2000 h or longer exhibited full discolouration. Compared to 0.5pH, the colour changes in FAGP exposed to 1pH acid solution show a progressive variation from 1000 to 3000 h of exposure, with FAGP-1pH-3000 h performing similarly to FAGP-0.5pH-1000 h. This phenomenon is confirmed by Gu et al. [21], where they reported colour change when geopolymer is exposed to 0.5pH (3%) sulphuric acid. At 4pH, FAGP specimens showed no discernible shift in colour or shape over the exposure period. Fig. 3 quantitatively depicts the percentage variance in weight loss (Fig. 3a) and associated diameter loss (Fig. 3b) of FAGP specimens. The results for weight and diameter changes in acid-deteriorated specimens represent the average of five specimens. The standard deviation is included in the graph; however, it is relatively small compared to the extensive range of the Y-axis, showing high consistency of the test results.

Significant physical changes occurred swiftly when OPC mortar specimens were subjected to highly acidic conditions (0.5pH and 1pH) as seen in Fig. 1b. Unlike FAGP, the acid reaction front for OPC appears to be at the perimeter, indicating that the deteriorated section has disintegrated from the sound matrix, resulting in diameter and mass loss (Fig. 3c and d). After 3000 h of exposure, OPC specimens at 0.5pH showed complete disintegration, whereas 1pH and 4pH showed 25% and 10% diameter loss (Fig. 3d). The corresponding FAGP values were 5, 2, and 1 (Fig. 3b). However, this is nonlinear with weight loss and may be attributable to ion leaching, as detailed in the next section.
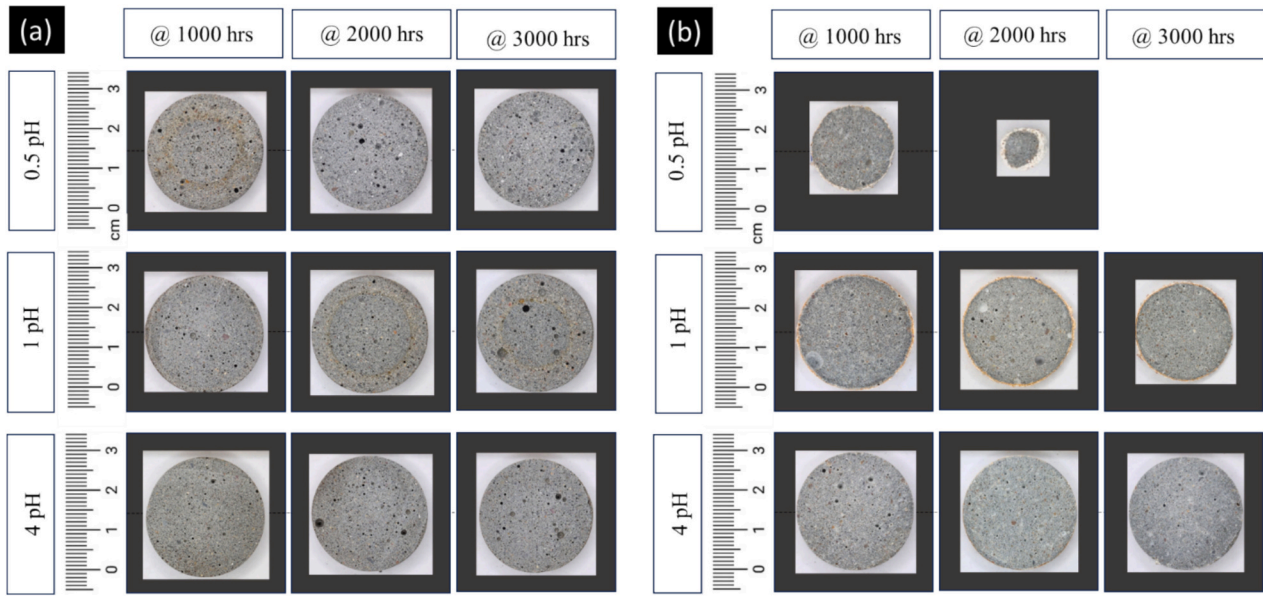
Fig. 2. Comparison of change in diameter of the acid deteriorated (a) FAGP and (b) OPC mortar specimens.
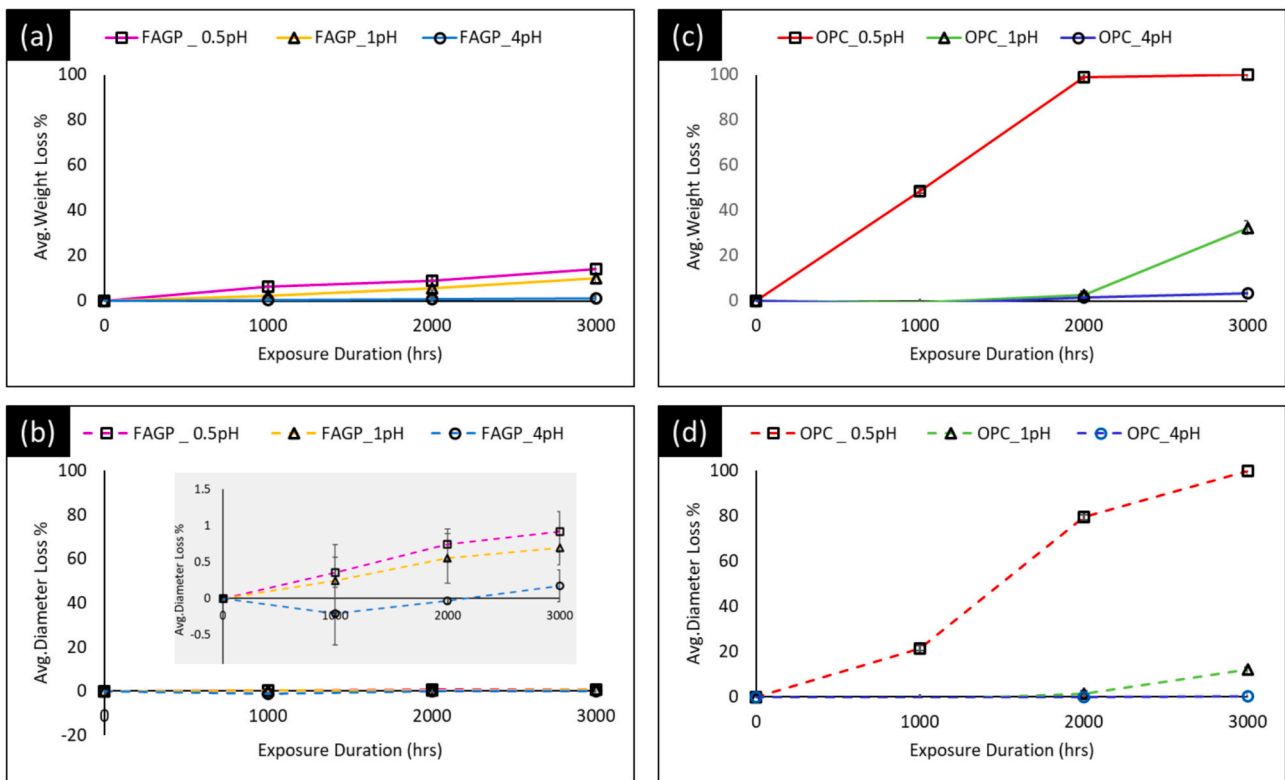

Fig. 3. Comparison of weight and diameter change in deteriorated (a-b) FAGP and (c-d) OPC mortar specimens

3.1.2. Surface change

Fig. 4 displays the surface changes observed through a stereo microscope at the reaction front of mortars exposed to sulphuric acid at concentrations of 0.5pH and 1pH following various exposure cycles, where (a) and (b) represent FAGP and OPC, respectively. When comparing the control samples (unexposed to acid solution), FAGP has no visual change, while OPC shows the effect of carbonation up to a depth of 300 μm from the sample edge, as estimated using the scale from the stereo-microscopic image of the discoloured surface. The 500 μm

scale in the figure was used as a reference to illustrate the depth of carbonation. According to Wells and Melchers [40], OPC carbonation starts early and drops the pH value to 10 or below, resulting in discolouration. When exposed to aggressive sulphuric acid (0.5pH), OPC samples revealed a considerable change in the mortar sample at the acid front.

The binder consumed by the acid turned into a soft white paste (assumed as gypsum), resulting in a roughened edge due to exposed aggregates. With increased exposure time, as seen in OPC_0.5pH_2000,
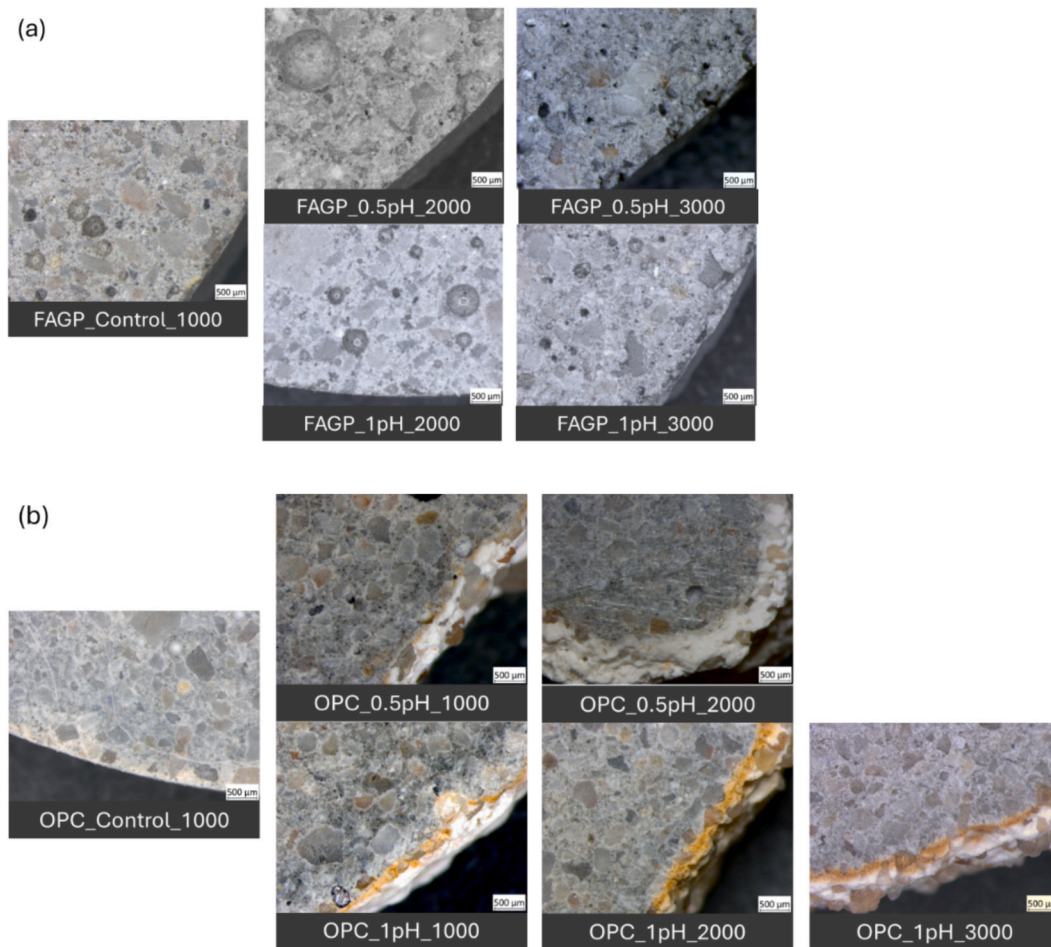
Fig. 4. A comparison of stereo microscopic images for surface change in mortar samples after different exposure cycles (a) FAGP and (b) OPC.

the thickness of the gypsum layer increases, and there is no obvious demarcation of the acid front. This can be attributed to the temporary impediment of acid contact caused by the thickened gypsum layer acting as a barrier until spalling occurs. With lower acid concentrations, the onset of OPC deterioration was delayed and advanced as exposure time increased, as evidenced in samples OPC_1pH_1000 to OPC_1pH_2000. In contrast, after 2000 h of acid corrosion exposure, FAGP_1pH exhibited no significant physical changes. After 3000 h of exposure, the binder seemed to partially dissolve in a strip up to 100 μm broad. This has been quantified in terms of mass and diameter loss, as illustrated in Figs. 3(a) and (b). Compared to 1pH, FAGP at 0.5pH sulphuric acid demonstrated a noticeable binder loss after 3000 h of exposure, further discussed in Section 3.4.2.

3.2. Residual mechanical properties

3.2.1. Compressive strength

Fig. 5 depicts the percentage residual mechanical strength in FAGP and OPC mortars exposed to sulphuric acid where (a) and (b) are for compressive strength results and (c) and (d) are for split tensile results, respectively. The percentage of residual mechanical strength was computed by subtracting the mechanical strength of the deteriorated mortar specimen from the initial strength and then multiplying the result by 100 to express it as a percentage. Under severe acidic conditions (at 0.5pH), FAGP and OPC experienced significant strength reduction. Nevertheless, FAGP retained 38% of its initial strength after 1000 h, which is approximately 15% higher than OPC. As seen in Fig. 5 (a), the rate of strength deterioration for FAGP-0.5pH did not differ significantly with increasing exposure time, with 35% residual strength

remaining after 3000 h. This is consistent with the ion leaching behaviour of FAGP_0.5pH, which is also observed in the phase transition. Under the 1pH acid condition, the compressive strength reduction for OPC increased exponentially from 9% to 60% with increased exposure duration, from 2000 h to 3000 h (Fig. 5(b)), whereas the FAGP response was from 10% to 22%. This coincides with OPC's diameter and mass loss at 1pH exposure conditions. FAGP subjected to 4pH acidic conditions showed an increase in strength of up to 20%, whereas the mechanical strength of OPC increased initially and then dropped by 20% at the end of the 3000 h cycle.

3.2.2. Splitting tensile strength

Fig. 5(c) shows that FAGP exposed to 0.5pH sulphuric acid lost approximately 40% of its splitting tensile strength during 1000 h of exposure, with an additional 20% loss at the end of 3000 h. In response, OPC (Fig. 5(d)) exhibited a similar reduction in strength during the initial 1000-h exposure phase. Additionally, specimens subjected to 0.5 pH sulphuric acid were completely dissolved by 2000 h of exposure. With decreased acid concentration, tensile strength increased in both mortar types, with 6% and 1% values in FAGP and OPC. As exposure length increased, tensile strength decreased to 15% and 53% at 3000 h in 1pH acid. At 4pH acid, both mortars showed an increase in tensile strength until 2000 h and then started to decline. Wardhono et al. [41] observed a considerable improvement in splitting tensile strength in FA-only geopolymer over time due to continuous geopolymerisation and contemporaneous gel formation, verified by a decrease in permeability parameters. However, a steady supply of H^+ ions into the system could have led the geopolymer matrix to release ions.
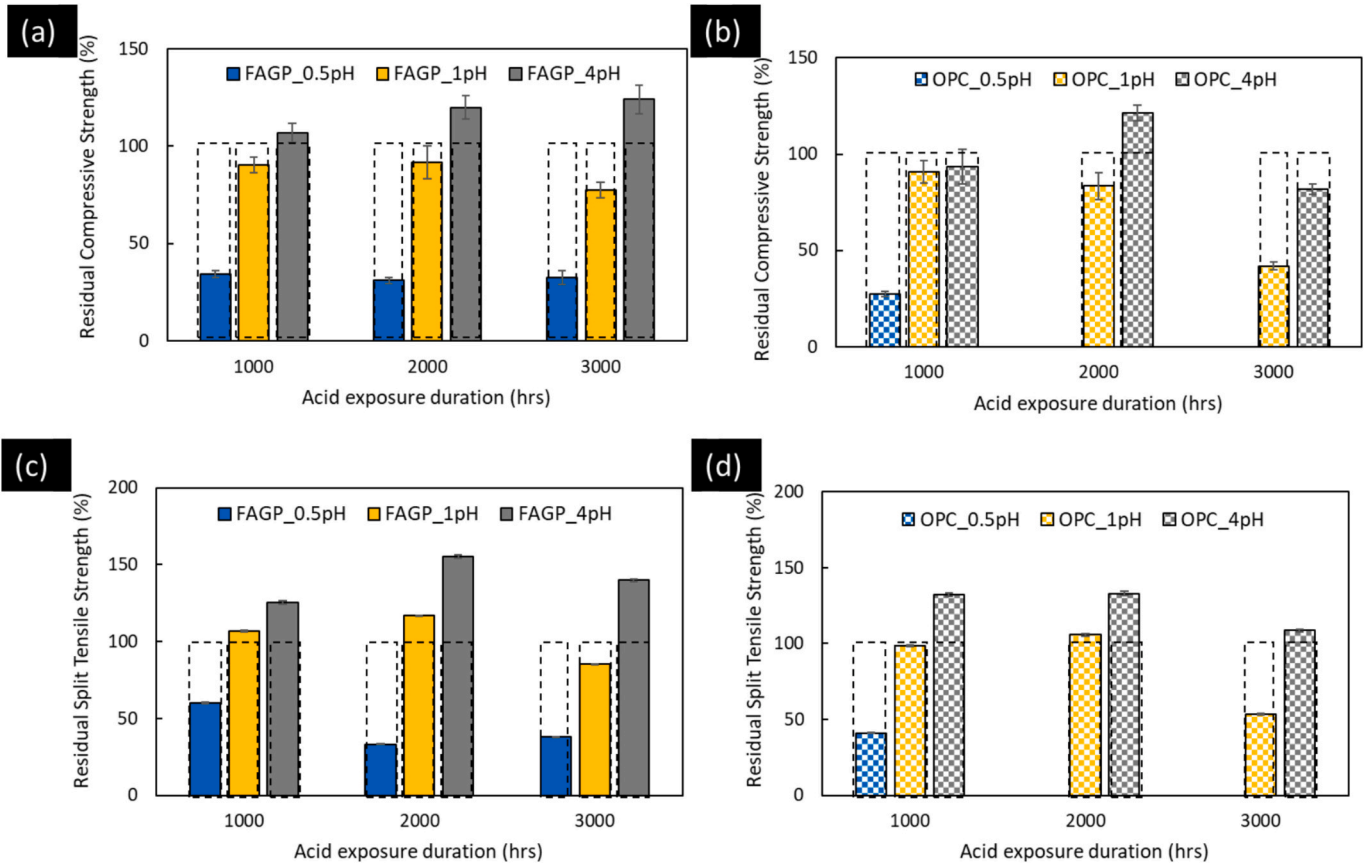
Fig. 5. Mechanical characterisation for residual strength: compressive (a) and (b) and split tensile (c) and (d) for FAGP and OPC mortars, respectively.
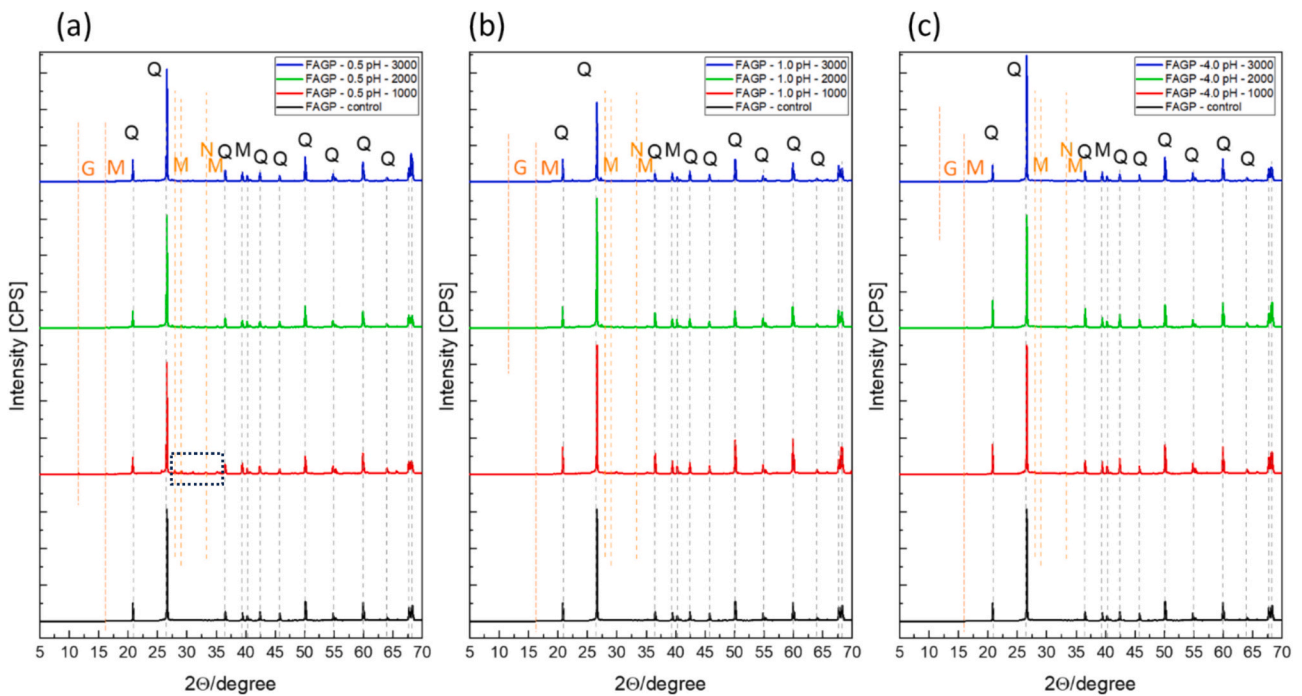

Fig. 6. XRD patterns of acid deteriorated FAGP mortar subjected sulphuric acid with various concentrations; (a) at 0.5pH, (b)at 1pH, and (c) at 4 pH (Q - Quartz, G-Gypsum, M - Mullite, N – Magnetite).

3.3. Phase transition

3.3.1. XRD

Fig. 5 shows the XRD patterns of acid-deteriorated repair mortars. Figs. 6 (a), (b), and (c) represent powder analysis of deteriorated outer skin of FAGP mortar specimens that were subjected to 0.5pH, 1pH and 4pH sulphuric acid, respectively. Each figure compares the XRD patterns of specimens after each exposure cycle. In all samples, crystalline quartz, present in the fine aggregate, was the predominant phase identified. Quartz was not removed from the XRD analysis to reflect the sample's true composition. Regardless of exposure duration, the sharp quartz peaks in all figures are similar to those in FAGP_Control, indicating minimal change in quartz content. This aligns with the substantial aggregate retention in the acid-deteriorated FAGP matrix, as shown by the modest diameter change after acid exposure.

The broad hump observed and highlighted in the box in FAGP XRD patterns between 25° and 35° 2θ indicates the presence of an amorphous or short-range organised structure [42,43]. The change in broadness and intensity of the hump reflects the degree of disorder and short-range arrangement in the substance. Minor, sporadic shifts in peak heights were observed in the amorphous region due to acid exposure; however, these shifts are not visible in the figures due to the applied scale, except in the FAGP-0.5pH XRD patterns (Fig. 6(a)), as indicated by the dotted area. Fig. 6(a) shows a minor gypsum ($CaSO_4$) peak, which could be attributable to a phase transition of accessible Ca in the fly ash binder. The emergence appeared to be delayed with decreasing acid concentrations. The stable peak intensity of gypsum throughout the exposure in FAGP_0.5pH may suggest formation inhibition due to the limited Ca^{2+} in the fly ash geopolymer binder and the low dissolution characteristic of gypsum in acid.

Mullite ($3Al_2O_3.2SiO_2$) is visible at 15° to 20° and 35° to 40° in all FAGP_0.5. It is an unreacted mineral that can be found in fly ash and, therefore, must be inherited from FAGP_Control [44]. Ge et al. [43] also reported that the unreacted aluminosilicate precursors cause the presence of Mullite in fly ash-based geopolymer. According to Temuujin et al. [45], these crystalline phases remain unaltered when exposed to acid, and the partial crystallisation on amorphous component surfaces promotes acid resistance in geopolymers. The next notable peak in FAGP was Magnetite (Fe_3O_4), an unreacted mineral typically contained in Fe-

rich precursors [46]. Magnetite (designated as N in the figure) peak intensities in FAGP (Figs. 6(a), (b) and (c)) showed no linearity with acid concentration or exposure period, which can be attributed to unreacted Fe ions from geopolymerisation that leached and precipitated in the acid-exposed area of the specimen [47].

Compared to FAGP mortar specimens, OPC exhibited substantial alterations in XRD patterns at the early stages of acid exposure, primarily corrosion products formed by the interaction of cementitious components with sulphuric acid (Fig. 7(a), (b) and (c)). Many researchers [20,21,24] have reported this behaviour. According to Wang et al. [10], the intensity of gypsum and ettringite peaks increased with the exposure time and the increased sulphuric acid concentrations. When Fig. 7(a) and (b) are compared, a modest drop in gypsum peak intensity is noticed, which could be attributed to gypsum reduction caused by spalling. Ettringite (Aft) peaks were found in Fig. 7(a), (b) and (c) in minor intensities, indicating dissolution due to its instability at pH < 10.

3.3.2. FTIR

Fig. 8 presents the FTIR spectra of FAGP and OPC mortar subjected to sulphuric acid corrosion with different acid concentrations of 0.5pH, 1pH, and 4pH compared to the unexposed counterpart. The analysis was conducted in the 4000 cm^{-1} to 400 cm^{-1} IR spectrum, with (a) and (b) representing FAGP and OPC, respectively, and (a') representing the zoomed-in FAGP spectra of the area represented by the dashed line box. Fig. 8(a) shows the distinctive vibrations in FAGP_Control spectra that occurred at various locations, including 1700–1300 cm^{-1}, 1300–900 cm^{-1}, and 900–800 cm^{-1}. Rożek et al. [48] support this, and they assign the centre band at approximately 1000 cm-1(1002 cm^{-1}) to Si—O (Si, Al) asymmetric stretching vibrations (Fig. 8(a')). This band appears to shift due to acid exposure, with FAGP_0.5pH wave numbers of 1080, 1095, and 1095 cm^{-1} at 1000-, 2000-, and 3000 h following exposure.

According to Alexander and Shashikala [49], shifts reflect microstructural change, and the intensity of this band is proportional to the reactivity of fly ash. The shift in the wave number decreases with lower acid concentrations, and no shift is observed at 4pH. This demonstrates that the microstructural evolution is a function of acid concentration and exposure duration and aligns with the XRD, MIP, and AAS results. The intensity of C—O stretching vibrations (about 1450 cm^{-1}) increases with increasing acid content and exposure period. However, the band in
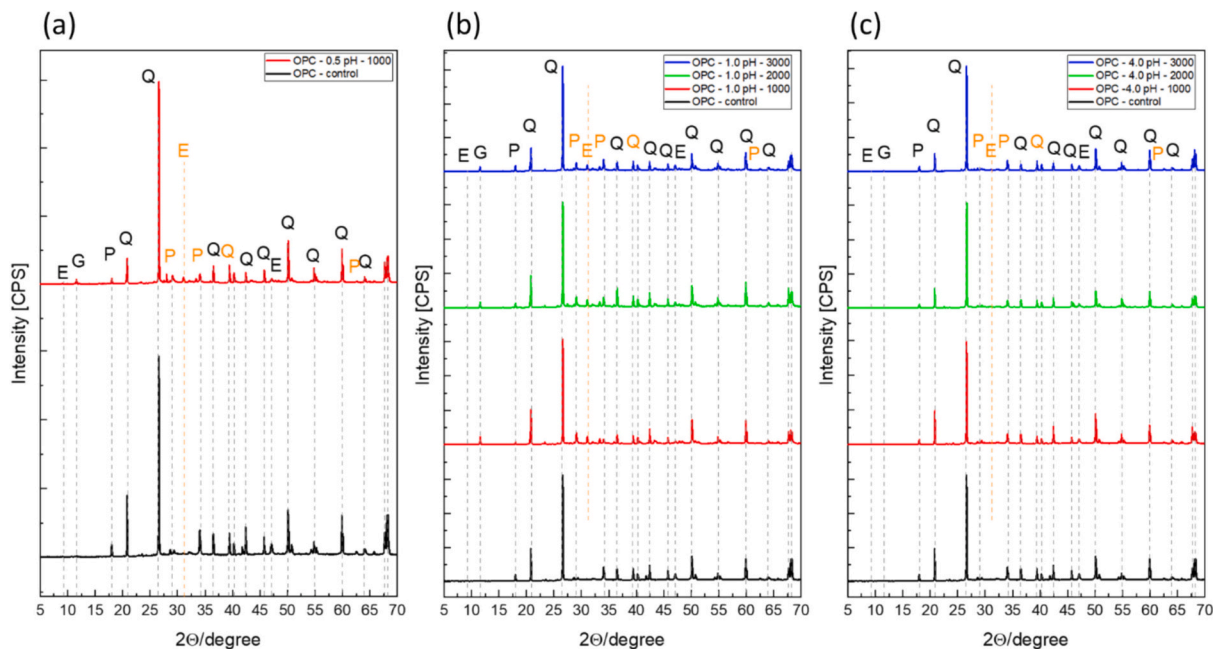

Fig. 7. XRD patterns of acid deteriorated OPC mortar subjected sulphuric acid with various concentrations; (a) at 0.5pH, (b)at 1pH, and (c) at 4 pH (Q - Quartz, G - Gypsum, E - Ettringite, P - Portlandite).
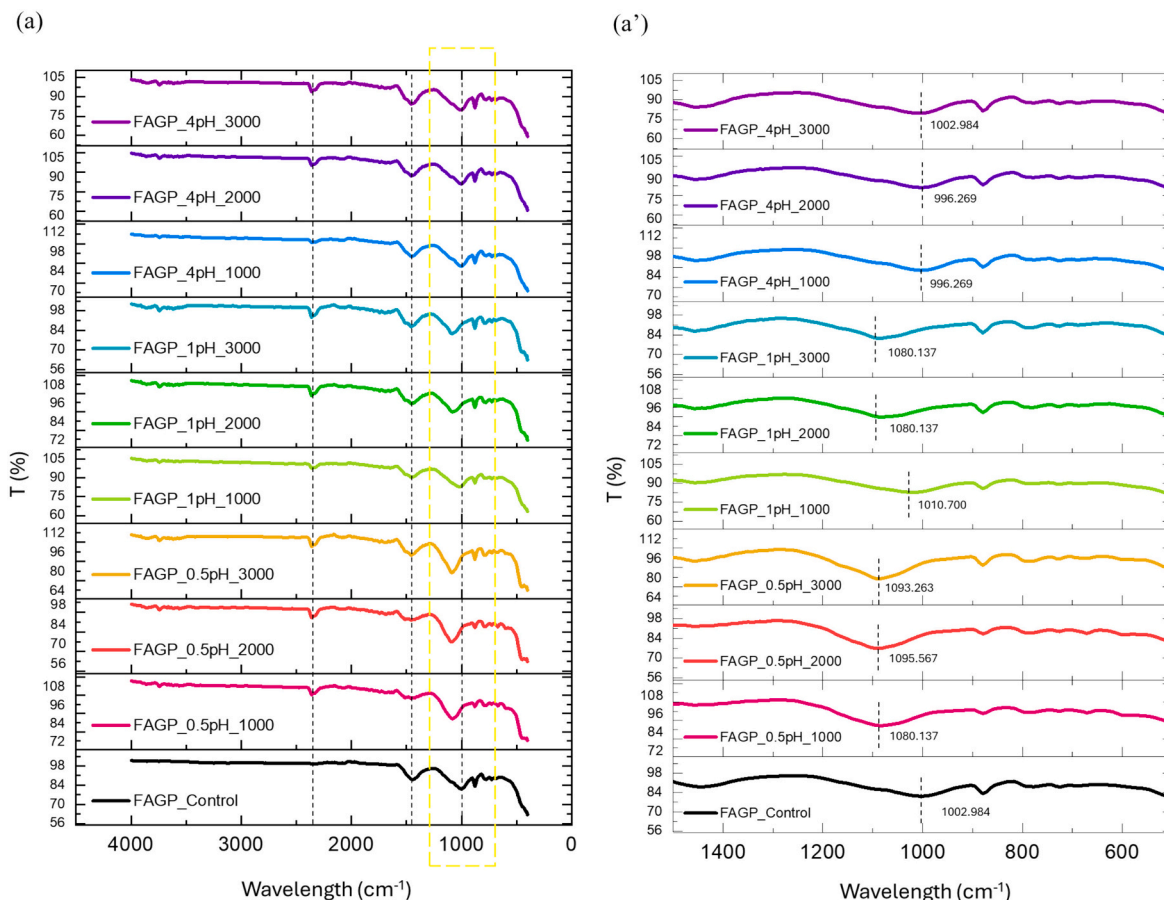
Fig. 8. (a) The FTIR spectra of FAGP at various sulphuric acid concentrations and exposure durations; (a') is the zoomed-in spectrum of the area represented in the dashed line box.

the 800–900 cm^{-1} region, which is symmetric Si-O-Si stretching vibration, remains almost unchanged. This is ascribed to the strong geopolymeric chain between the fine aggregate and the N-A-S-H gel in the FAGP, as evidenced by microscopic images, even after acid deterioration [50]. Similarly, only a modest change to the Al—O bending vibration, i.e. in the range 600–800 cm^{-1}, is visible due to acid corrosion, as described by Rożek et al. [48] and Ali et al. [12]. Valencia-Saavedra et al. [51] discovered an increase in the band intensity of FA/GGBFS geopolymer in this range when exposed to sulphuric acid, which could be attributed to the presence of Ca^{2+} in the GGBFS, which interacts with $1\,M\,H_2SO_4$ over 180 days. The current study utilised low-calcium fly ash, thus rendering this explanation inapplicable. When comparing the variations in the 0.5pH, 1pH, and 4 pH with the FAGP_Control counterpart, followed by the acid corrosion, it is noticed that a formation of new bands can be found in wavenumbers 3700–3800 cm^{-1} and 2300–2400 cm^{-1}, where the former is due to the OH groups of Si-OH and adsorbed water molecules [52]. A distinctive peak appeared at 1621 cm^{-1} in the sulphuric acid-exposed FA-geopolymer spectra, identified by Bai et al. [50] as the presence of gypsum, was not observed in FAGP in this study due to the absence of Ca^{2+} in the FA aluminosilicate precursor.

Fig. 8(b) depicts the FTIR spectra of OPC at various sulphuric acid concentrations after 3000 h of exposure. These spectra differ from those of FAGP. The Si—O asymmetric vibration at 530 cm^{-1}, corresponding to C-S-H gel [50], weakened with increasing acid concentration. A similar trend was observed in the O—H stretching vibration at 3700–3800 cm^{-1}, corresponding to portlandite, albeit at lower intensities. Furthermore, the characteristic peak of OPC-Control at 1100 cm^{-1} appeared altered in terms of peak heights under acid corrosion,

suggesting the conversion of anhydrite (AFm) to ettringite [30]. This observation is consistent with the phase transition of OPC assessed by XRD data, discussed in Section 3.3.1.

3.4. Pore structure characteristics

The performance of a repair material is highly dependent on its internal pore structure, which is classified into two types: intrinsic and extrinsic. Intrinsic pores naturally form during the initial formation or crystallisation of the material and are thus inherently part of its structure. In contrast, extrinsic pores indicate secondary changes in the material, often resulting from environmental exposure or applied stress. Geopolymers have unique pore structures influenced by various parameters, including aluminosilicate precursor composition, alkali activator dosage, liquid-to-binder ratio, and curing procedure, and their changes in response to service conditions vary accordingly [53]. Non-uniformly distributed unreacted or semi-reacted fly ash cenospheres may increase mean pore size and total porosity in FA-geopolymers compared to Ca-rich geopolymers. Zhang et al. [54] and Wang et al. [55] found that fly ash particle size and shape affect pore structure; smaller particles promote alkali reactivity and denser packing, which inhibits foreign matter entry into the matrix.

3.4.1. MIP analysis
The pore evolution of mortars due to acid immersion was assessed using MIP analysis. Fig. 9 depicts the porosity evolution of representative mortar samples after exposure to sulphuric acid, with (a), (b), and (c) representing FAGP mortar specimens exposed to acid concentrations of 0.5 pH, 1 pH, and 4 pH, respectively. The specimen porosity examined
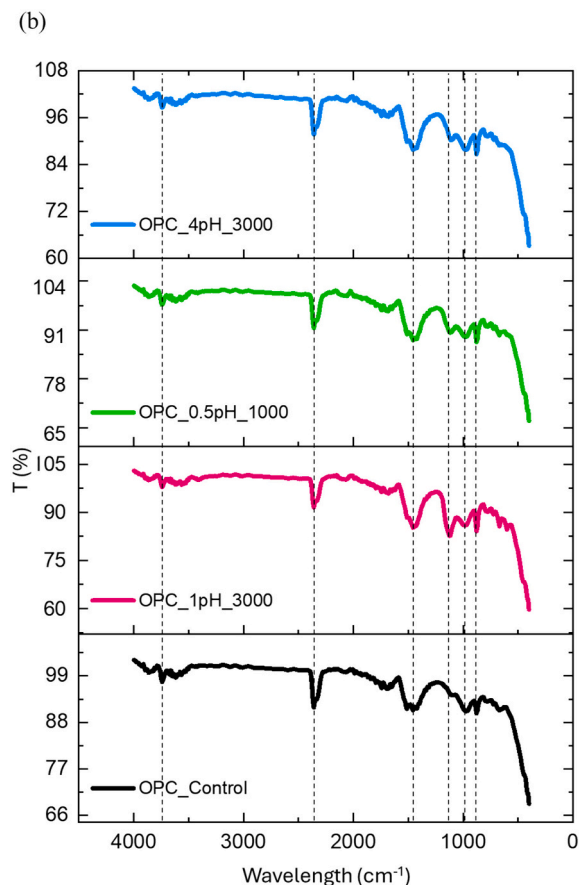
(b)

Fig. 8. (b) The FTIR spectra of OPC at various sulphuric acid concentrations and exposure durations.

at each exposure duration was compared to the unexposed sample in each figure. In Fig. 9(a), it is evident that the pore structure of the geopolymer matrix has evolved, resulting in a matrix of increased pore diameters, specifically between 0.05 and 10 μm, replacing the gel pores due to aggressive acid corrosion. This can be attributed to ion leaching from the N-A-S-H gel, which makes the matrix porous. Fu et al. [29] and Temuujin et al. [45] suggest that the acid resistance of geopolymers is contingent upon their mineral composition and the reactivity of fly ash. Hematite, magnetite, and maghemite in fly ash are not involved in geopolymerisation, so they are susceptible to acid corrosion, which results in leaching out from the matrix. A similar tendency was detected with FAGP specimens immersed in 1pH sulphuric acid (Fig. 9(b)), albeit with less intensity. Specimens exhibiting FAGP_4pH showed the most negligible change in pore structure when compared to specimens immersed in 0.5 and 1pH sulphuric acid, and it was discovered that pores <0.01 μm increased considerably while pores between 0.1 and 10 μm decreased over 1000 h of exposure (Fig. 9(c)). This is attributed to the lack of minimal acidic conditions necessary to dissolve aluminium from the FAGP matrix [29]. However, when exposure increased, the percentage of gel pores diminished, and the micropores expanded.

Fig. 9(d) shows that the gel pores in the unexposed matrix in OPC mortar reduced with increasing acid concentration and prolonged acid attack. However, the results for pores in the macro-region, as shown in Fig. 9(d), were implausible. This phenomenon might be due to the spalling of extremely porous gypsum, also observed in XRD data.

Fig. 10 summarises the porosities of the mortar matrixes normalised to 100%. The pores are classified as gel pores <0.01 μm, micropores between 0.01 and 1 μm and *meso* and macro capillary pores >1 μm. Compared to unexposed FAGP, OPC showed 10% more gel pores without macrocapilary pores. This suggests that the FAGP mortar pore

structure is more responsive to acid transport into the matrix than OPC [6]. Wang et al. [56] observed an approximately linear relationship between the capillary water absorption coefficient and pore structure with diameters in the range of 10-1000 nm. However, Amran et al. [57] contested this, discovering reduced porosity in geopolymer concrete (synthesised with FA + GGBS) compared to standard concrete as evaluated by the water absorption rate. They attributed this to FA's finer particle size compared to OPC. Fig. 10 depicts a clear pore evaluation regardless of acid concentration, with gel pores being reduced in both FAGP and OPC binders. FAGP_0.5pH_1000 has comparable pore content to FAGP_1pH_3000, with a 40% decrease in gel pores and a 45% increase in micropores and macrocapilary pores as compared to FAGP_Control. In contrast, no significant change was observed in FAGP mortars immersed in 4pH sulphuric acid after 1000 h. However, results after 2000 h showed a decreasing tendency of macrocapillary pores. This can be attributed to the improved geopolymerisation under mildly acidic conditions, which fills pores and increases strong matrices, as revealed in post-acid characterisation for mechanical strength. This is consistent with the findings of Gunasekara et al. [58], who found continuous geopolymerisation in fly ash-based geopolymers in 365 days of pore evolution: the reactivity of partially reacted and unreacted fly ash results in precipitating as aluminosilicate gel products, reducing macro- and mesopores. During the third phase of the exposure, FAGP_4pH macropores reappeared due to geopolymer matrix disintegration from prolonged exposure. OPC_4pH showed a progressive decline in gel pores with exposure duration.

3.4.2. SEM analysis

Fig. 11 shows the SEM micrographs of the FAGP mortar subjected to 0.5pH sulphuric acid for 1000 h. (a)—(d) represents the selected zones in the acid-deteriorated zone, and (e) shows a point in the unexposed zone at different magnifications. The acid front displays a distinct colour alteration. The area corroded by acid exhibits a slightly greater exposure of fine aggregates than the unexposed zone, indicating that the matrix has been dissolved. This phenomenon is likely associated with the removal of Al, Na, and Fe ions from the N-A-S-H gel within the geopolymer matrix [28]. This aligns with the modest mass change that occurred in FAGP_0.5pH_1000 discussed previously. Fig. 11(a) and (b) illustrate the intrinsic pores formed during this process. The latter exhibits a crystalline phase of sodium sulphate, indicating that sulphate ingress leads to the transformation of the aluminosilicate gel. Despite the aggressive exposure conditions, the aggregate interfacial transition zone (ITZ) appears unaffected, as no cracks are visible in the adjoining area (Fig. 11(c)). A similar observation has also been made by Gu et al. [20]. The partially reacted FA particles display microcracks but remain embedded within the geopolymer matrix (Fig. 11(d)). The boundary delineating the two zones can be interpreted as the depth of acid neutralisation, as illustrated in Fig. 11(e), with the region to the right of the boundary revealing a heterogeneous matrix, thus confirming the presence of the unexposed core.

The deterioration of OPC under sulphuric acid exposure is primarily attributed to chemical damage induced by the reaction of C-S-H and portlandite within the cementitious matrix with sulphate ions in the presence of high H^+ concentrations [34]. Numerous studies [35,59,60] have extensively documented the severity of this attack over the years. Fig. 12 illustrates the acid-exposed OPC mortar sample, with the acid front indicated in yellow. After 1000 h in 0.5 pH sulphuric acid, the outer skin of the mortar specimen suffered significant deterioration, leading to the formation of a structure with extrinsic pores, as depicted in Fig. 12(a) and (a'). Upon closer inspection, abandoned gypsum ($CaSO_4.2H_2O$) crystals can be observed, contributing to the expansion of the cementitious structure and the formation of micro-fissures, ultimately resulting in material spalling [61]. Fig. 12(b) and (b') illustrate an area anticipated to be exposed to acid, demonstrating the extension of microcracks, indicating the onset of corrosion.
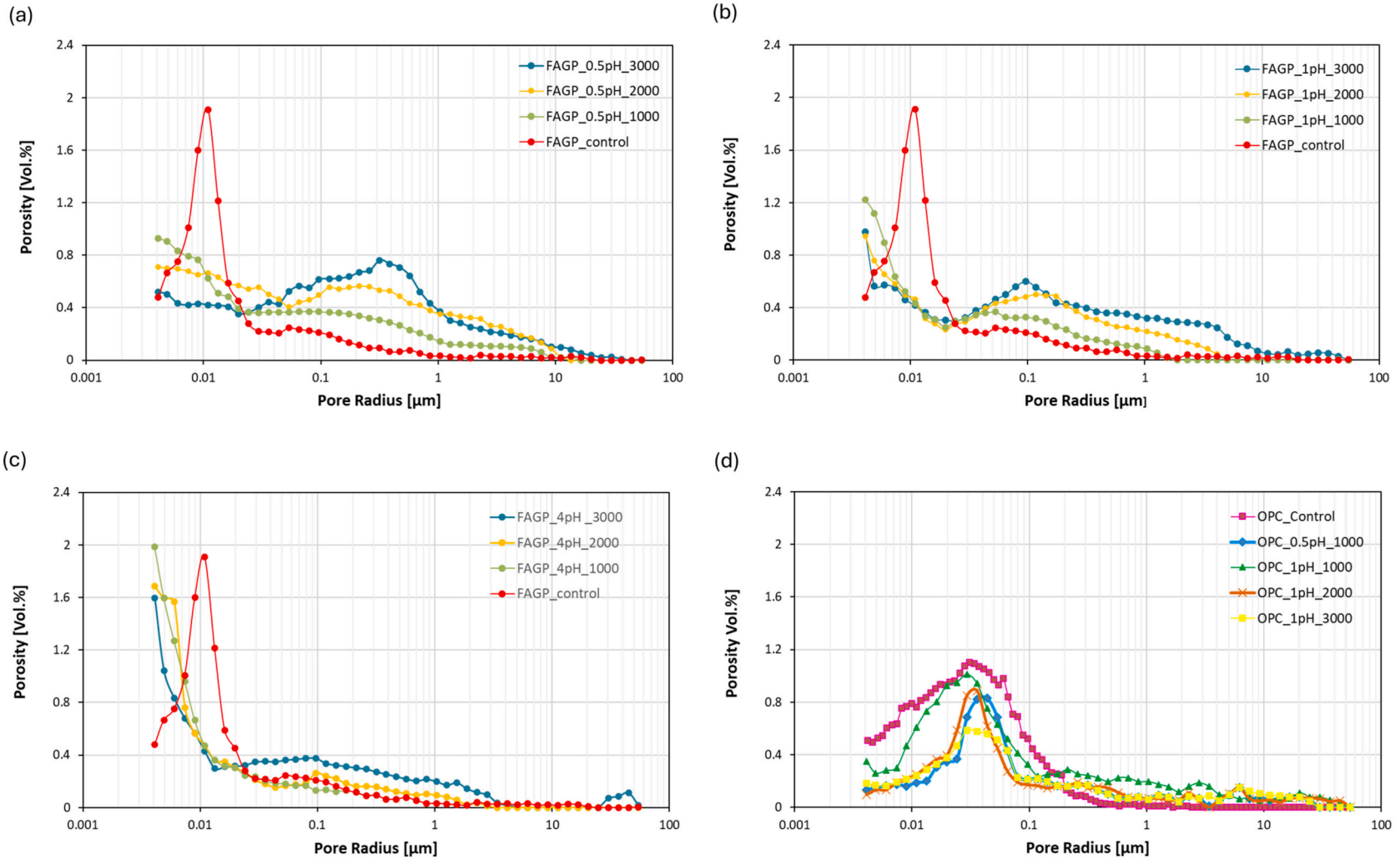
(a)

(b)

(c)

(d)

Fig. 9. MIP results for the pore evolution of acid- acid-deteriorated mortars; (a) – (c) FAGP and (d) OPC.
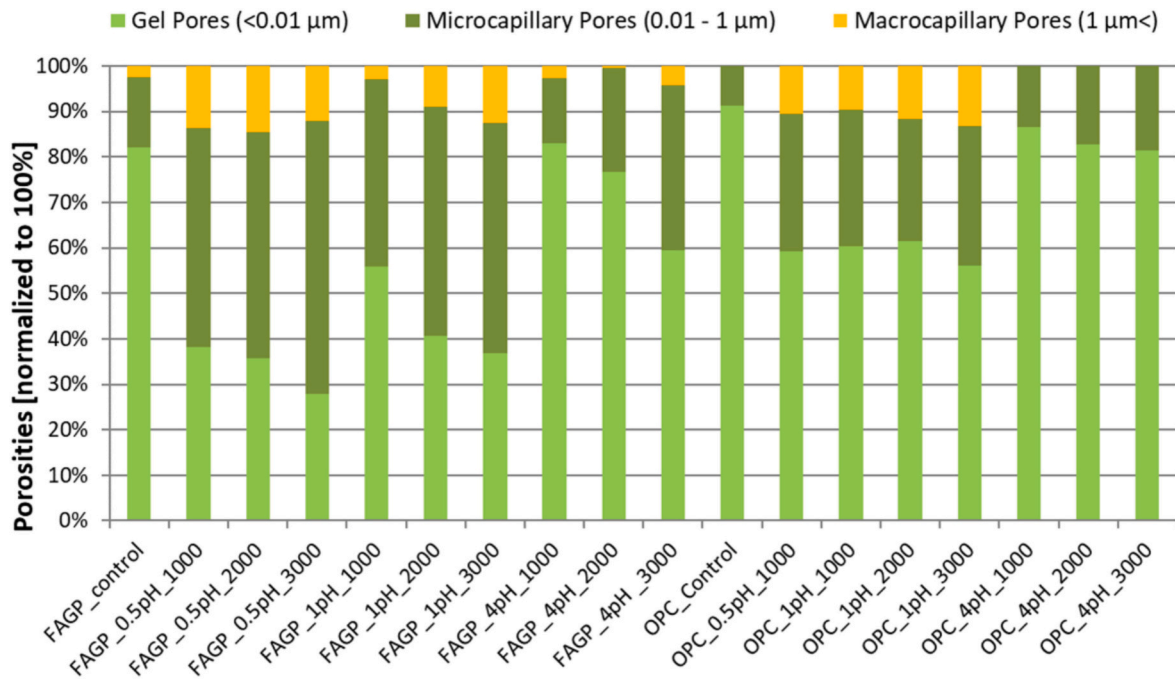
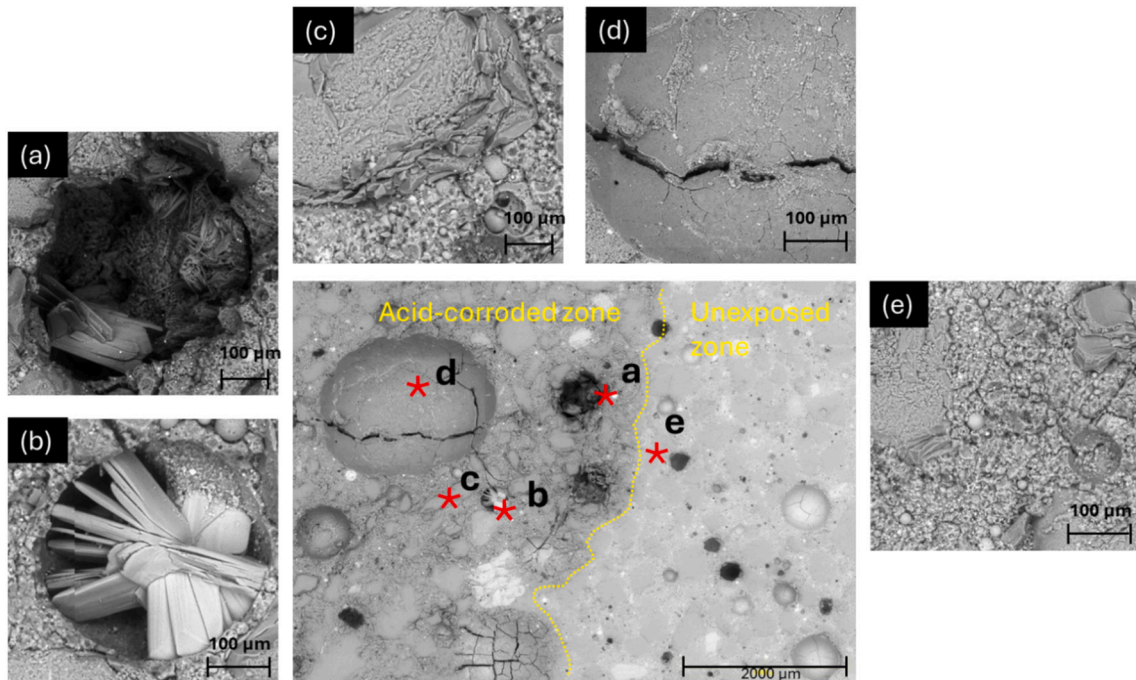**Fig. 10.** Comparison of FAGP and OPC mortar porosities, normalised to 100%,

Fig. 11. SEM micrographs of FAGP_0.5pH_2000.

3.5. Ion diffusion/leaching

3.5.1. Elemental mapping

Figs. 13 and 14 illustrate the distribution of elements in FAGP and OPC mortars exposed to sulphuric acid attack. EDS mapping was used to investigate the qualitative aspects of element adsorption and leaching. The distribution of calcium (Ca), sulphur (S), aluminium (Al), iron (Fe), and silicon (Si) elements was specially chosen for investigation. Fig. 13 (a) illustrates the element distribution of unexposed FAGP. Compared to the unexposed sample with the FAGP_0.5pH counterparts (as shown in

Fig. 13(b-i)), there is a reduction in the Ca^{2+} ions in the outer region after 1000 h of exposure. The sulphur intrusion zone appears to coincide with this, demonstrating the extent of damage. The reaction rate slowed during the second exposure phase, as shown in Fig. 13(b-ii), with Ca^{2+} ions in the core disintegrating and exiting the matrix, as seen in Fig. 13 (b-iii). At the end of 2000 h of exposure, a complete sulphur intrusion was observed, which then appeared to diminish, starting with the outermost region of the FAGP specimen. Lavigne et al. [62] and Kiliswa et al. [63] have corroborated the observation in Fig. 13(b) that the diminution in Al and Fe ions increases with exposure time. A slight
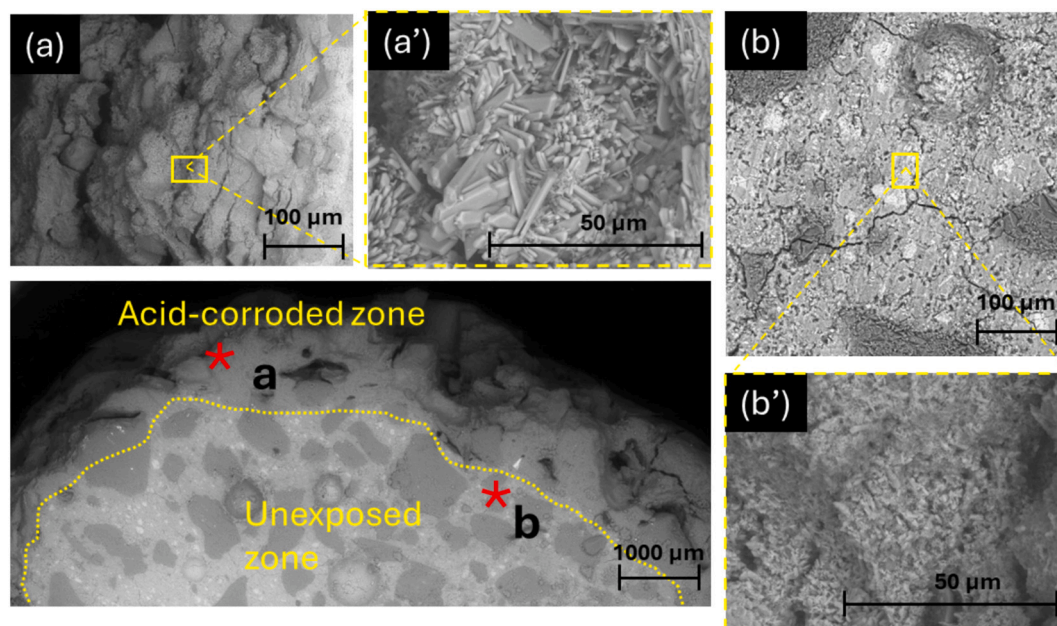
Fig. 12. SEM micrograph of OPC_0.5pH_2000 at different magnifications

change in the silicon distribution is evident after 3000 h of exposure compared to the FAGP_Control. This explains the residual integrity of the geopolymer gel and the fine aggregates that maintain the matrix in shape. As seen in Fig. 13(c), the rate of ion dissolution and transport caused by geopolymer-acid interaction diminished with low acid concentrations. However, the process continued with extended exposure. The effect of Ca^{2+} dissolution and sulphur ingress in FAGP_1pH after 3000 h (Fig. 13(c-ii)) was less than in FAGP_0.5pH after 1000 h. Even after 3000 h of exposure to 4pH sulphuric acid, there was no apparent ion transfer, consistent with the XRD findings in Section 3.3.1.

Compared to OPC_Control (Fig. 14(a)), the elemental distribution of OPC mortars caused by acid attack (Figs. 14b, c and d) showed minimal to no alteration in Ca^{2+} ion density on the examined specimen cross-section. A narrow band of sulphur is visible in the outermost region of OPC_0.5pH_1000 (as seen in Fig. 14(b-i and b-ii)). This phenomenon was observed in specimens subjected to different acid concentrations and durations of exposure, irrespective of the remaining cross-sectional area of the sample (Figs. 14c and d). This is due to the calcium silicate hydrate (C-S-H) and portlandite reactivity with H^+ from sulphuric acid, which begins with Ca dissolution and progresses through gypsum formation, expansion, and spalling. Although gypsum synthesis accelerates with increasing acid concentration and exposure duration, the spalling of expanded corrosion products distorts the sulphur distribution in the outer region. Unlike in FAGP, OPC mortar deterioration was demonstrated to occur even at 4pH (Fig. 14(d)). As reported by Madraszewski et al. [17], the cement matrix's stability is compromised by the dissolution of calcium hydroxide (CH) at pH <12.5, followed by C-S-H dissolution and Ca^{2+} leaching.

3.5.2. Ion leachate

Free Ca^{2+} and Al^{3+} ions in the leachate during the acid exposure were examined to determine the effects of sulphuric acid attack. Fig. 15 graphically displays the Atomic Absorption Spectrometry analysis findings for FAGP and OPC mortars.

3.5.2.1. Calcium.
Fig. 15(a) shows the calcium concentrations in the FAGP leachate collected at the end of each immersion cycle. The highest calcium leachate amount was seen at a pH level of 0.5 during the initial 1000 h and at a level between 400 and 500 ppm. By the end of 2000 and 3000 h, the Ca fraction in the leachate reduced to below 200 ppm. This

phenomenon is caused by the quick movement of calcium ions to the surface when there are high concentrations of H^+ ions in the solution, followed by a slowdown due to a shortage of calcium ions in the substance. When the pH level was one or higher, the calcium leachate for FAGP was consistently <50 ppm in each cycle.

Fig. 15(b) shows that the accessible free calcium in OPC leachate varied significantly with time, regardless of acid concentration. OPC reported a count of <200 ppm Ca ions for the first 1000 h, which grew threefold during the subsequent 1000-h cycle before decreasing marginally. This can be primarily due to the development of gypsum and ettringite, which absorbed most Ca^{2+} ions leached out from the cementitious matrix, leaving a low level in the solution. Unlike most other salts, gypsum has retrograde solubility. It is moderately soluble at 25 °C and less soluble at higher temperatures. As time progresses, gypsum and ettringite formation equilibrium results in more free-accessible Ca^{2+} ions in the leachate. With lower acid concentrations (pH levels 1 and 4), free accessible Ca^{2+} appeared lower than higher concentrations during the early phase. This could be attributed to slow ion transfer because of the low concentration of H^+ ions. However, an increase in free-accessible Ca^{2+} was observed in the later stages due to the inhibition of calcium salt production at lower pH levels.

3.5.2.2. Aluminium leachate.
A significant quantity of Al^{3+} ions in the leachate was visible in FAGP when exposed to 0.5 pH sulphuric acid (Fig. 15(c)). At the end of the first stage (0−1000h), the Al leachate of FAGP was 1126.14 ppm, which increased by 22% during the second stage (1000−2000h). Subsequently, the leaching process was decelerated, and the aluminium concentration in the leachate was quantified at 718.56 ppm from 2000 to 3000 h. This behaviour agrees with the experimental results published by Wang et al. [64]. They noticed a steep inclination of increasing aluminium leachate from the aluminosilicate binder (NASH) paste treated to 5% (pH < 0.5) sulphuric acid for the first 30 days (~ 720 h) at a cumulative concentration of 35×10^3 ppm. Then, the leaching rate is reduced, followed by a decrease in the leaching rate. The prominent N-A-S-H gel in low calcium geopolymers is a three-dimensional alkali-aluminosilicate hydrate gel network with terminal hydroxyl groups on the surface of crosslinked $[AlO_4]$ and $[SiO_4]$ tetrahedra joined by oxygen atoms. When subjected to acid, the aluminium ions leach out of the NASH gel, leaving a silicon-rich structure. This supports Fig. 1 in Section 3.1.1, which shows a modest change in the
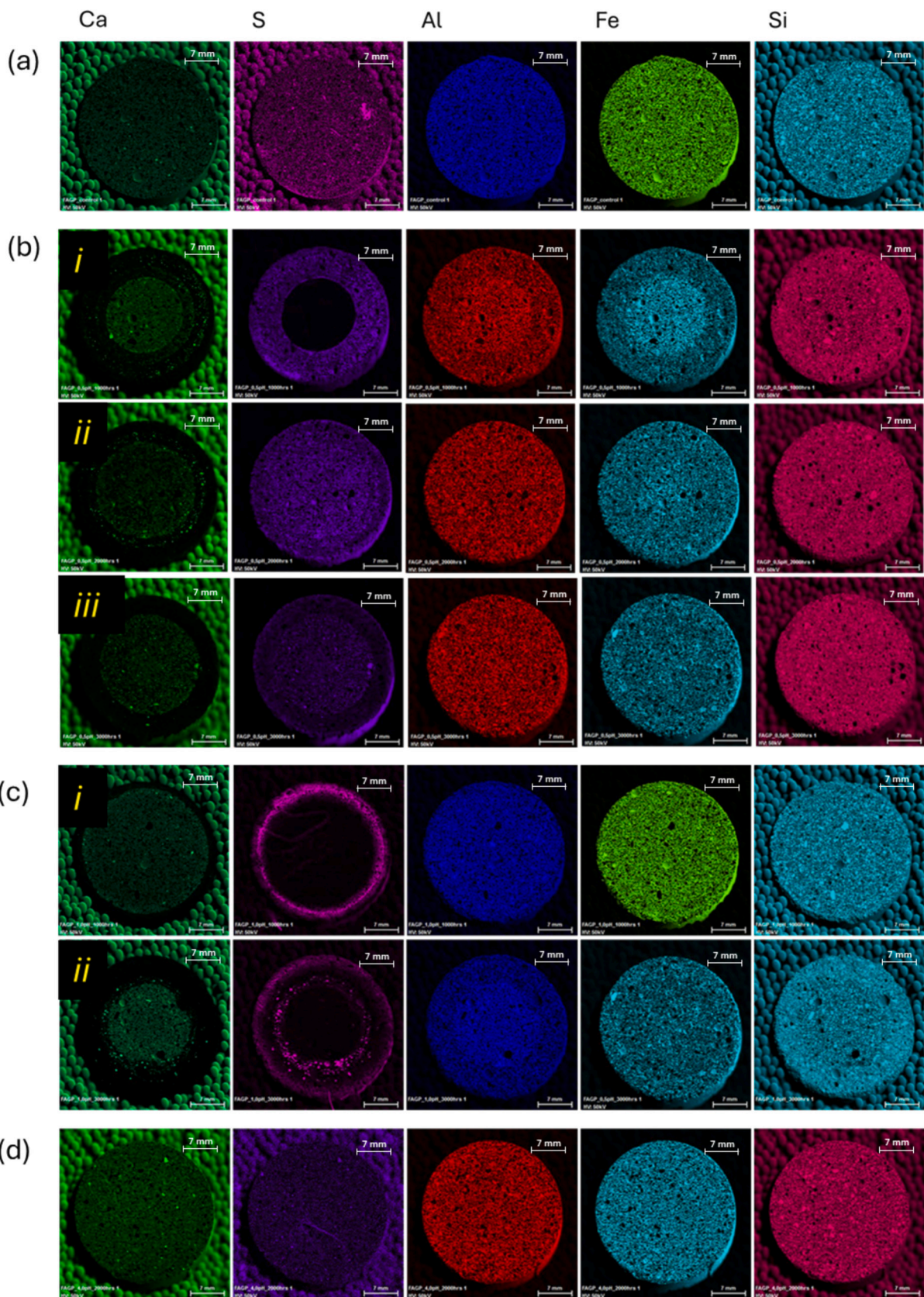
Fig. 13. Elemental mapping for calcium (Ca), sulphur(S), aluminium (Al), ferrous (Fe) and silicon(*Si*)in FAGP mortars; (a) unexposed, (b), (c) and (d) are for acid exposed at 0.5pH, 1pH and 4pH, respectively (i-iii represents 1000–3000 h exposure cycles).

Fig. 14. Elemental mapping for calcium (Ca), sulphur(S), aluminium (Al), ferrous (Fe) and silicon(*Si*)in OPC mortars; (a) unexposed, (b), (c) and (d) are for acid exposed at 0.5pH, 1pH and 4pH, respectively (i-ii represents 1000–2000 h exposure cycles).
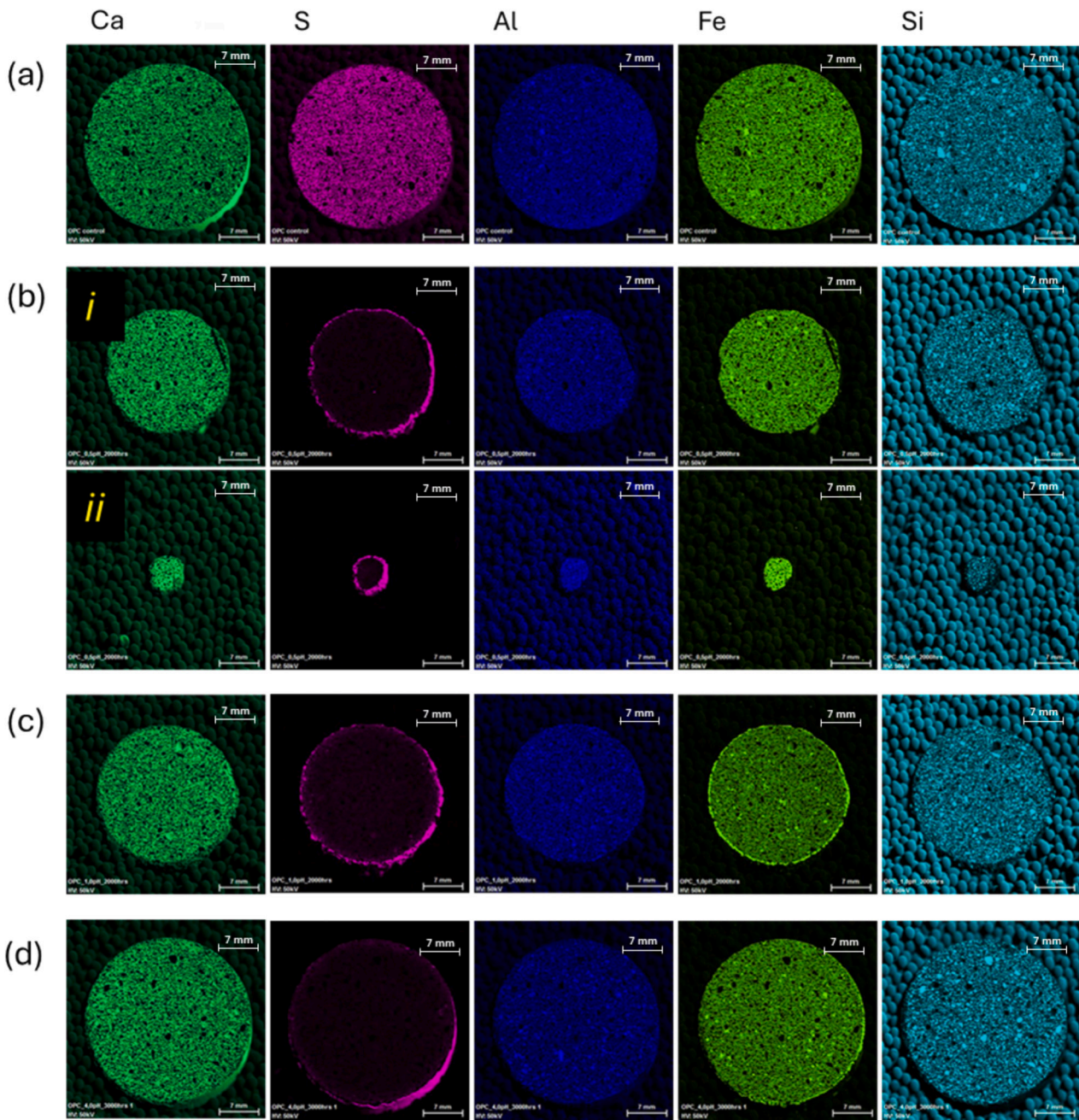
FAGP specimen cross-section even after exposure to aggressive acidic conditions.

According to Damion and Chaunsali [19], the increased release of aluminium has a favourable impact on reducing biogenic concrete deterioration. The bacteriostatic effect is caused by positively charged aluminium ions reacting with bacterial cell walls, resulting in osmotic cell instability. OPC leachate at 0.5pH exhibits a comparable tendency, albeit with a 60% lower count than the FAGP equivalent (Fig. 15(d)). The release of aluminium ions from the mortar matrix was impeded at low pH levels. In response to a 1 pH acidic environment, FAGP and OPC yielded 773.39 ppm and 135.51 ppm of Al^{3+} in the leachate, respectively. Compared to the second 1000-h period, FAGP showed a rise in aluminium leachate during the following phase of exposure, which was also observed in OPC. At 4pH sulphuric acid, aluminium ion release from OPC was minimal, <200 ppm, which aligns with the elemental mapping data.

4. Conclusion

This study examined the resilience of a low-calcium FA-based geopolymer repair mortar under laboratory-simulated typical sewer conditions. The FAGP mortar specimens and their OPC counterparts were immersed in Sulphuric acid of varying concentrations to replicate moderate to highly corrosive sewer conditions. The resulting chemo-transport damage was periodically evaluated using visual observations, mass/cross-section changes, residual mechanical strength, ion stability, and pore structure changes.

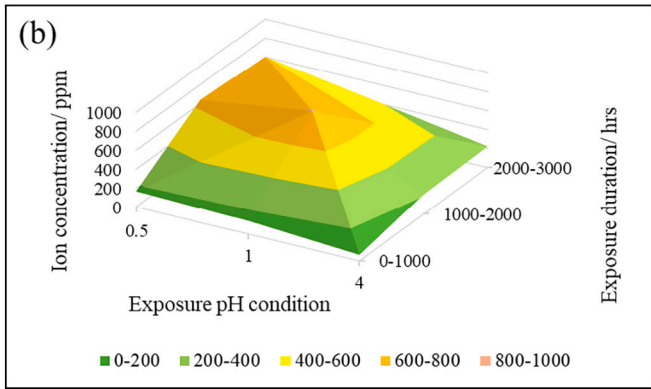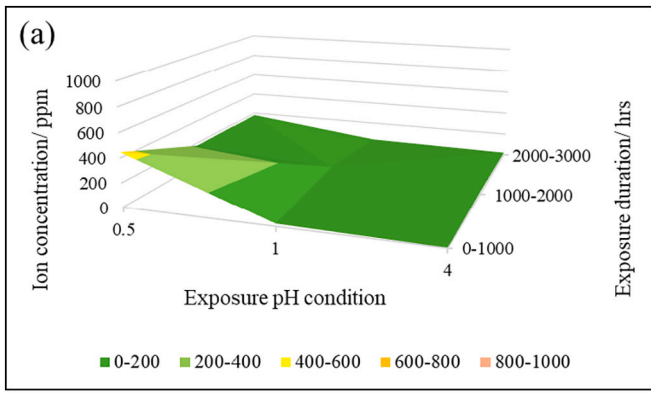The following conclusions can be drawn:

Fig. 15. (a–b). Calcium ion leaching occurred in (a) FAGP and (b) OPC repair mortars at varied acid solution concentrations during each exposure.
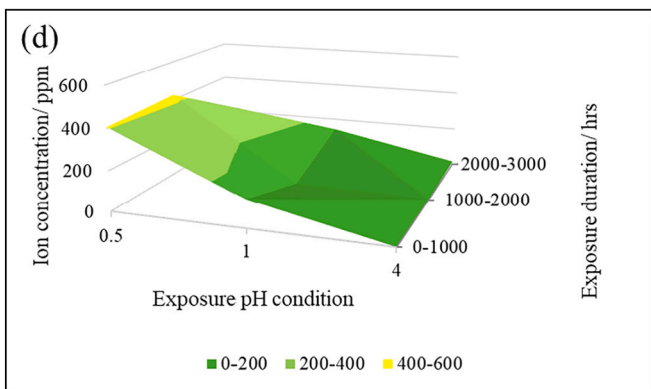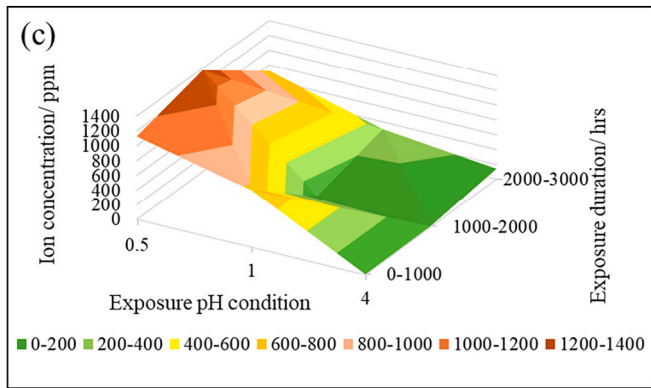

Fig. 15. (c–d). Aluminium ion leaching occurred in (c) FAGP and (d) OPC repair mortars at varied acid solution concentrations during each exposure.

1) FAGP is more resilient than OPC in aggressive sewer conditions. FAGP mortars exposed to acid corrosion exhibited limited changes in weight and dimensions: only around 15% and <1.5%, respectively, in highly acidic conditions (0.5 pH) over 3000 h. In contrast, OPC experiences rapid deterioration with 94% weight loss at 2000 h and complete failure thereafter. Chemical damage is apparent at lower acid concentrations where OPC exhibits gradual cross-section reduction and localised damage at the specimen periphery, while FAGP shows discolouration in affected areas, indicating ion transfer but maintaining structural integrity. Neither OPC nor FAGP shows visual alteration in 4pH acid after 3000 h.

2) The structural integrity of the OPC mortar can significantly decline in severe sewer conditions. Similarly, FAGP can experience a decrease in compressive strength with 0.5pH acid but can maintain >30% of its mechanical strength in subsequent exposure stages. This resilience can be attributed to reduced corrosion damage pace, possibly due to the absence of reactive substances or the slowing of transport mechanisms through pore filling by precipitated corrosion products. At pH >1, both FAGP and OPC mortar experienced a surge in strength, likely attributed to the sustained progression of geopolymerisation and cementation processes. However, their structural strength gradually declined with prolonged exposure, albeit slower for FAGP than OPC.

3) XRD and FTIR analyses revealed a correlation between the phase transition of repair mortars due to sulphuric acid corrosion and associated physical and mechanical alterations. Acid-damaged FAGP exhibited only modest changes compared to unexposed samples, suggesting minimal chemical reactions during the corrosion process. There is also a robust geopolymeric chain between the fine aggregate and the N-A-S-H gel in the FAGP. Conversely, OPC samples displayed significant gypsum and ettringite development, with variations in peak heights in the 1500 cm^{-1} and 1200–1400 cm^{-1} FTIR spectra associated with C—O and Si-O-Si stretching vibrations, respectively.

4) MIP characterisation unveiled that unexposed FAGP contained about 18% capillary pores, with microcapillary pores to macrocapillary pores in an 8:1 ratio. Upon exposure to 0.5pH acid, macro capillary pores initially increased, then decreased and were replaced by microcapillaries. This pore size reduction likely limited acid penetration into deeper layers. In contrast, in OPC, a notable portion of gel pores transitioned into capillary pores due to the formation of expansive gypsum and ettringite upon sulphuric acid exposure, facilitating heightened acid ingress. The observed pore evolution in FAGP and OPC is influenced by acid concentration and exposure duration.

5) FAGP_0.5pH and FAGP_1pH exhibited a surge in Al ion leach out during the early stages of the acid exposure, followed by a subsequent decrease towards the end. There is also a decline in Al distribution density in the outer region compared to the unexposed core. The strength of this shift is inversely correlated with the decrease in acid concentration but directly correlated with the exposure duration. In contrast, OPC showed minimal Al dissolution but notable calcium depletion from the matrix in the form of gypsum and ettringite. Sulphur ingress in FAGP appeared to rise with exposure duration, with its distribution density proportional to acid concentration. However, the measured value was significantly lower than that in OPC, indicating decreased capillary pores in the FAGP matrix. Furthermore, the mobilisation of Fe ions is evident in the deteriorated zone of FAGP from acid exposure, contrasting with the OPC counterpart, which is obscured by the spalling of the deteriorated zone.

This study offers insights into the degradation of low-calcium geopolymer mortar, assessed across physical, mechanical, microstructural, and chemical stability parameters under laboratory-induced sewer conditions mimicking real-world scenarios. While the structural integrity loss of FAGP is attributed to ion leaching, the observed enhanced

impermeability under low acid concentrations remains unexplained. It warrants further investigation into identifying complex corrosion products and their impact on pore structure. This study is limited to a comparison of XRD patterns between the specimen groups; however, an in-depth analysis of the acid-exposed zones, in terms of phase identification and quantification, is required for a precise understanding of the phase evolution process. Developing a simplified theoretical/empirical formula to predict FAGP mortar deterioration, based on interpreting experimental results regarding material loss and residual mechanical properties under varying sewer conditions, is also considered beneficial for assessing geopolymer as a potential repair material for sewer pipe rehabilitation.

CRediT authorship contribution statement

Piumika W. Ariyadasa: Writing – original draft, Validation, Methodology, Investigation, Formal analysis, Data curation, Conceptualization. **Allan C. Manalo:** Writing – review & editing, Validation, Supervision, Resources, Methodology, Conceptualization. **Weena Lokuge:** Writing – review & editing, Validation, Supervision. **Vasantha Aravienthan:** Writing – review & editing, Validation, Supervision. **Andreas Gerdes:** Writing – review & editing, Supervision, Resources. **Jonas Kaltenbach:** Writing – review & editing, Investigation, Data curation.

Declaration of competing interest

There is no conflict of interest.

Acknowledgement

Data availability

All data used are reported in the manuscript.

References

[1] J. Marchand, E. Samson, Predicting the service-life of concrete structures – limitations of simplified models, Cement and Concrete Composites 31 (8) (2009) 515–521.

[2] A. Mehta, R. Siddique, Sulfuric acid resistance of fly ash based geopolymer concrete, Construct. Build Mater. 146 (2017) 136–143.

[3] T.A. Aiken, L. Gu, J. Kwasny, G.F. Huseien, D. McPolin, W. Sha, Acid resistance of alkali-activated binders: a review of performance, mechanisms of deterioration and testing procedures, Construct. Build Mater. 342 (2022) 128057.

[4] M. Berndt, Evaluation of coatings, mortars and mix design for protection of concrete against Sulphur oxidising bacteria, Construct. Build Mater. 25 (10) (2011) 3893–3902.

[5] F. Pacheco-Torgal, Z. Abdollahnejad, S. Miraldo, S. Baklouti, Y. Ding, An overview on the potential of geopolymers for concrete infrastructure rehabilitation, Construct. Build Mater. 36 (2012) 1053–1058.

[6] P.W. Ariyadasa, A.C. Manalo, W. Lokuge, V. Aravinthan, A. Gerdes, J. Kaltenbach, B.A. Galvan, Macro and microstructural evolution of low-calcium fly ash-based geopolymer mortar exposed to sulphuric acid corrosion, Cem. Concr. Res. 178 (2024) 107436.

[7] S. Qin, D. Zou, T. Liu, A. Jivkov, A chemo-transport-damage model for concrete under external sulfate attack, Cem. Concr. Res. 132 (2020) 106048.

[8] A.A. Aliabdo, A.M. Abd Elmoaty, M.F. Mohamed, Permeability indices and corrosion resistance of geopolymer and Portland cement concretes, Mag. Concr. Res. 70 (12) (2018) 595–609.

[9] M. Wu, T. Wang, K. Wu, L. Kan, Microbiologically induced corrosion of concrete in sewer structures: a review of the mechanisms and phenomena, Construct. Build Mater. 239 (2020) 117813.

[10] T. Wang, K. Wu, L. Kan, M. Wu, Current understanding on microbiologically induced corrosion of concrete in sewer structures: a review of the evaluation methods and mitigation measures, Construct. Build Mater. 247 (2020) 118539.

[11] H. Khan, M. Yasir, A. Castel, Performance of cementitious and alkali-activated mortars exposed to laboratory simulated microbially induced corrosion test, Cement and Concrete Composites 128 (2022) 104445.

[12] H.A. Ali, D. Xuan, J.-X. Lu, C.S. Poon, Enhancing the resistance to microbial induced corrosion of alkali-activated glass powder/GGBS mortars by calcium aluminate cement, Construct. Build Mater. 341 (2022) 127912.

[13] I. Luhar, S. Luhar, A comprehensive review on Fly ash-based Geopolymer, Journal of Composites Science 6 (2022) 219.

[14] A. Bertron, Understanding interactions between cementitious materials and microorganisms: a key to sustainable and safe concrete structures in various contexts, Materials and Structures 47 (11) (2014) 1787–1806.

[15] M.G. Alexander, C. Fourie, Performance of sewer pipe concrete mixtures with Portland and calcium aluminate cements subject to mineral and biogenic acid attack, Mater. Struct. 44 (1) (2011) 313–330.

[16] L.J. Kong, W.J. Zhao, D.X. Xuan, X.B. Wang, Y.Z. Liu, Application potential of alkali-activated concrete for antimicrobial induced corrosion: a review, Construct. Build Mater. 317 (2022).

[17] S. Madraszewski, F. Dehn, J. Gerlach, D. Stephan, Experimentally driven evaluation methods of concrete sewers biodeterioration on laboratory-scale: a critical review, Construct. Build Mater. 320 (2022) 126236.

[18] H. Khan, A. Castel, M. Khan, Performance Evaluation of Geopolymer against in Situ Aggressive Sewer Environment, 2017.

[19] T. Damion, P. Chaunsali, Biogenic acid resistance of calcium sulfoaluminate cement: revelations from a field study, Cement and Concrete Composites 145 (2024) 105324.

[20] L. Gu, T. Bennett, P. Visintin, Sulphuric acid exposure of conventional concrete and alkali-activated concrete: assessment of test methodologies, Construct. Build Mater. 197 (2019) 681–692.

[21] L. Gu, P. Visintin, T. Bennett, Evaluation of accelerated degradation test methods for cementitious composites subject to sulfuric acid attack: application to conventional and alkali-activated concretes, Cement and Concrete Composites 87 (2018) 187–204.

[22] H. Khan, A. Castel, M.S.H. Khan, A.H. Mahmood, Durability of calcium aluminate and sulphate resistant Portland cement based mortars in aggressive sewer environment and sulphuric acid, Cem. Concr. Res. 124 (2019) 105852.

[23] T. Gourley, G. Johnson, The Corrosion Resistance of Geopolymer Concrete Sewer Pipe. 43 (2019) 38–44.

[24] M. Albitar, M.M. Ali, P. Visintin, M. Drechsler, Durability evaluation of geopolymer and conventional concretes, Construct. Build Mater. 136 (2017) 374–385.

[25] H.A. Khan, A. Castel, M.S.H. Khan, Corrosion investigation of fly ash based geopolymer mortar in natural sewer environment and sulphuric acid solution, Corros. Sci. 168 (2020).

[26] S. T, K.R. P. R, S. M, S. A, J. R, *A state-of-the-art on development of geopolymer concrete and its field applications.* Case studies in Constr. Mater., 2022. 16: p. e00812.

[27] C. Grengg, N. Ukrainczyk, G. Koraimann, B. Mueller, M. Dietzel, F. Mittermayr, Long-term in situ performance of geopolymer, calcium aluminate and Portland cement-based materials exposed to microbially induced acid corrosion, Cem. Concr. Res. 131 (2020) 106034.

[28] H.A. Khan, M.S.H. Khan, A. Castel, J. Sunarho, Deterioration of alkali-activated mortars exposed to natural aggressive sewer environment, Construct. Build Mater. 186 (2018) 577–597.

[29] Q. Fu, W. Xu, X. Zhao, M. Bu, Q. Yuan, D. Niu, The microstructure and durability of fly ash-based geopolymer concrete: a review, Ceram. Int. 47 (21) (2021) 29550–29566.

[30] H. Ye, L. Huang, Degradation mechanisms of alkali-activated binders in sulfuric acid: the role of calcium and aluminum availability, Construct. Build Mater. 246 (2020) 118477.

[31] S. John, Y. Nadir, G. K, Effect of Source Materials, Additives on the mechanical properties and durability of Fly ash and Fly ash-slag Geopolymer mortar: a review, Construct. Build Mater. (2021) 280.

[32] K. Arbi, M. Nedeljkovic, Y. Zuo, G. Ye, A review on the durability of alkali-activated fly ash/slag systems: advances, issues, and perspectives, Ind. Eng. Chem. Res. 55 (19) (2016) 5439–5453.

[33] N. Zhang, A. Hedayat, L. Figueroa, K.X. Steirer, H. Li, H.G. Bolaños Sosa, R. P. Huamani Bernal, N. Tupa, I.Y. Morales, R.S. Canahua Loza, Experimental studies on the durability and leaching properties of alkali-activated tailings subjected to different environmental conditions, Cement and Concrete Composites 130 (2022) 104531.

[34] C. Grengg, F. Mittermayr, N. Ukrainczyk, G. Koraimann, S. Kienesberger, M. Dietzel, Advances in concrete materials for sewer systems affected by microbial induced concrete corrosion: a review, Water Res. 134 (2018) 341–352.

[35] H. Yuan, P. Dangla, P. Chatellier, T. Chaussadent, Degradation modelling of concrete submitted to sulfuric acid attack, Cem. Concr. Res. 53 (2013) 267–277.

[36] T. Wells, R.E. Melchers, Modelling concrete deterioration in sewers using theory and field observations, Cem. Concr. Res. 77 (2015) 82–96.

[37] P. Wells, R.E. Melchers, Microbial corrosion of sewer pipe in Australia-initial field results, in: In *18th International Corrosion Congress Proceedings November*, Citeseer, 2011.

[38] ASTM International, ASTMC109 Standard Test Method for Compressive Strength of Hydraulic Cement Mortars (Using 2-in. or 50-mm cube specimens), S&P Global. p. (1983) 8.

[39] ASTM International, *ASTMC496/C496M Standard Test Method for Splitting Tensile Strength of Cylindrical Concrete Specimens.* 2017, S&P Global. p. 5.

[40] T. Wells,R. Melchers. *Findings of a 4 year study of concrete sewer pipe corrosion.* in *Annual Conference of the Australasian Corrosion Association.* 2014.

[41] A. Wardhono, C. Gunasekara, D.W. Law, S. Setunge, Comparison of long term performance between alkali activated slag and fly ash geopolymer concretes, Construct. Build Mater. 143 (2017) 272–279.

[42] G.S. Ryu, Y.B. Lee, K.T. Koh, Y.S. Chung, The mechanical properties of fly ash-based geopolymer concrete with alkaline activators, Construct. Build Mater. 47 (2013) 409–418.

[43] X. Ge, X. Hu, C. Shi, The effect of different types of class F fly ashes on the mechanical properties of geopolymers cured at ambient environment, Cement and Concrete Composites 130 (2022) 104528.

[44] F. Qu, W. Li, K. Wang, S. Zhang, D. Sheng, Performance deterioration of fly ash/slag-based geopolymer composites subjected to coupled cyclic preloading and sulfuric acid attack, J. Clean. Prod. 321 (2021) 128942.

[45] J. Temuujin, A. Minjigmaa, M. Lee, N. Chen-Tan, A. van Riessen, Characterisation of class F fly ash geopolymer pastes immersed in acid and alkaline solutions, Cem. Concr. Compos. 33 (10) (2011) 1086–1091.

[46] X. Wu, X. Zhou, C. Guo, D. Kang, W. Zhang, J. Lan, Z. Fang, Behavior of hematite, magnetite, and reduced iron powder in geopolymers: effects of mechanical properties and reaction mechanism, J. Clean. Prod. 444 (2024) 141178.

[47] J.S.J. van Deventer, J.L. Provis, P. Duxson, G.C. Lukey, Reaction mechanisms in the geopolymeric conversion of inorganic waste to useful products, J. Hazard. Mater. 139 (3) (2007) 506–513.

[48] P. Rożek, M. Król, W. Mozgawa, Spectroscopic studies of fly ash-based geopolymers, Spectrochim. Acta A Mol. Biomol. Spectrosc. 198 (2018) 283–289.

[49] A.E. Alexander, A.P. Shashikala, Studies on the microstructure and durability characteristics of ambient cured FA-GGBS based geopolymer mortar, Construct. Build Mater. 347 (2022) 128538.

[50] Y. Bai, W. Guo, Q. Zhao, N. Zhang, C. Xue, S. Wang, Y. Song, Performance deterioration of municipal solid waste incineration fly ash-based geopolymer under sulfuric acid attack, Construct. Build Mater. 391 (2023) 131847.

[51] W.G. Valencia-Saavedra, R. Mejía de Gutiérrez, F. Puertas, Performance of FA-based geopolymer concretes exposed to acetic and sulfuric acids, Construct. Build Mater. 257 (2020) 119503.

[52] S. Alehyen, M. Achouri, M. Taibi, Characterization, microstructure and properties of fly ash-based geopolymer, J. Mater. Environ. Sci 8 (5) (2017) 1783–1796.

[53] S. Chen, S. Ruan, Q. Zeng, Y. Liu, M. Zhang, Y. Tian, D. Yan, Pore structure of geopolymer materials and its correlations to engineering properties: a review, Construct. Build Mater. 328 (2022) 127064.

[54] M. Zhang, H. Xu, A.L. Phalé Zeze, X. Liu, M. Tao, Coating performance, durability and anti-corrosion mechanism of organic modified geopolymer composite for marine concrete protection, Cement and Concrete Composites 129 (2022) 104495.

[55] Y. Wang, Y. Cao, Z. Zhang, P. Zhang, Y. Ma, A. Wang, H. Wang, Intrinsic sulfuric acid resistance of C-(N)-A-S-H and N-A-S-H gels produced by alkali-activation of synthetic calcium aluminosilicate precursors, Cem. Concr. Res. 165 (2023) 107068.

[56] Y. Wang, L. Li, M. An, Y. Sun, z. yu, H. Huang, Factors influencing the capillary water absorption characteristics of concrete and their relationship to pore structure. Appl. Sci., 2022. 12: p. 2211.

[57] M. Amran, A. Al-Fakih, S.H. Chu, R. Fediuk, S. Haruna, A. Azevedo, N. Vatin, Long-term durability properties of geopolymer concrete: An in-depth review, Case Studies in Construction Materials 15 (2021) e00661.

[58] C. Gunasekara, D.W. Law, S. Setunge, Long term permeation properties of different fly ash geopolymer concretes, Construct. Build Mater. 124 (2016) 352–362.

[59] S. Wei, Z. Jiang, H. Liu, D. Zhou, M. Sanchez-Silva, Microbiologically induced deterioration of concrete: a review, Braz. J. Microbiol. 44 (4) (2013) 1001–1007.

[60] X. Li, F. Khademi, Y. Liu, M. Akbari, C. Wang, P.L. Bond, J. Keller, G. Jiang, Evaluation of data-driven models for predicting the service life of concrete sewer pipes subjected to corrosion, J. Environ. Manage. 234 (2019) 431–439.

[61] G. Jiang, J. Keller, P.L. Bond, Determining the long-term effects of H2S concentration, relative humidity and air temperature on concrete sewer corrosion, Water Res. 65 (2014) 157–169.

[62] M.P. Lavigne, A. Bertron, C. Botanch, L. Auer, G. Hernandez-Raquet, A. Cockx, J.-N. Foussard, G. Escadeillas, E. Paul, Innovative approach to simulating the biodeterioration of industrial cementitious products in sewer environment. Part II: validation on CAC and BFSC linings, Cem. Concr. Res. 79 (2016) 409–418.

[63] M.W. Kiliswa, K.L. Scrivener, M.G. Alexander, The corrosion rate and microstructure of Portland cement and calcium aluminate cement-based concrete mixtures in outfall sewers: a comparative study, Cem. Concr. Res. 124 (2019) 105818.

[64] Y. Wang, Y. Cao, Z. Zhang, J. Huang, P. Zhang, Y. Ma, H. Wang, Study of acidic degradation of alkali-activated materials using synthetic C-(N)-A-S-H and N-A-S-H gels, Compos. Part B Eng. 230 (2022) 109510.